MICROCOPY RESOLUTION TEST CHART
NATIONAL BUREAU OF STANDARDS-1963-A

AD-A171 990

⑫

CHARACTERIZATION OF MECHANICAL DAMAGE MECHANISMS IN CERAMIC COMPOSITE MATERIALS

By
James Lankford, Jr.

For
Office of Naval Research
Arlington, VA 22217
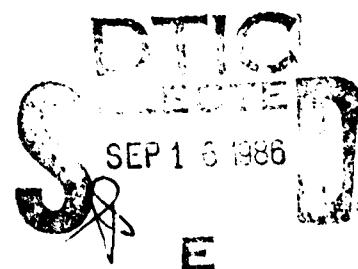
By
Southwest Research Institute
San Antonio, Texas

DTIC FILE COPY

July 1986

SEP 1 6 1986

E
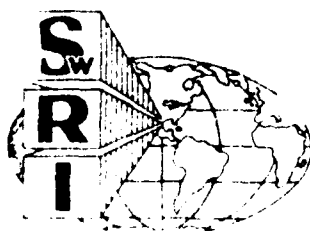
SOUTHWEST RESEARCH INSTITUTE
SAN ANTONIO   HOUSTON

REPORT DOCUMENTATION PAGE

1a. REPORT SECURITY CLASSIFICATION	1b. RESTRICTIVE MARKINGS
Unclassified	

2a. SECURITY CLASSIFICATION AUTHORITY	3. DISTRIBUTION/AVAILABILITY OF REPORT
2b. DECLASSIFICATION/DOWNGRADING SCHEDULE	Distribution Unlimited

4. PERFORMING ORGANIZATION REPORT NUMBER(S)	5. MONITORING ORGANIZATION REPORT NUMBER(S)
06-8124	NR 032-553

6a. NAME OF PERFORMING ORGANIZATION	6b. OFFICE SYMBOL (If applicable)	7a. NAME OF MONITORING ORGANIZATION
Southwest Research Institute		Dr. Steven G. Fishman - Code 431N Office of Naval Research

6c. ADDRESS (City, State and ZIP Code)	7b. ADDRESS (City, State and ZIP Code)
6220 Culebra Road, P.O. Drawer 28510 San Antonio, TX 78284	800 North Quincy Street Arlington, VA 22217

8a. NAME OF FUNDING/SPONSORING ORGANIZATION	8b. OFFICE SYMBOL (If applicable)	9. PROCUREMENT INSTRUMENT IDENTIFICATION NUMBER
Office of Naval Research		N00014-84-C-0123

8c. ADDRESS (City, State and ZIP Code)	10. SOURCE OF FUNDING NOS			
800 North Quincy Street Arlington, VA 22217	PROGRAM ELEMENT NO	PROJECT NO.	TASK NO.	WORK UNIT NO.

11. TITLE (Include Security Classification) Characterization of Mechanical Damage Mechanisms in Ceramic Composite Materials

12. PERSONAL AUTHOR(S)
James Lankford

13a. TYPE OF REPORT	13b. TIME COVERED	14. DATE OF REPORT (Yr., Mo., Day)	15. PAGE COUNT
Technical	FROM 5/24/85 TO 5/23/86	July 1986	

16. SUPPLEMENTARY NOTATION

17	COSATI CODES		18. SUBJECT TERMS (Continue on reverse if necessary and identify by block number) Key Words
FIELD	GROUP	SUB. GR.	Compressive strength; partially stabilized zirconia; tempera-ture effects; composite materials; fracture mechanisms; ceramics; plastic flow; glass matrix ceramics; cavitation

19. ABSTRACT (Continue on reverse if necessary and identify by block number)

Yielding behavior and deformation modes are characterized for single crystal and poly-crystalline yttria-stabilized ZrO_2 tested in compression from 23C to 800C. The plastic flow of single crystal specimens is orientation and temperature dependent, and is interpreted in terms of TEM evidence of dislocation activity, and an hypothesized tetragonal-to-cubic transformation. Polycrystalline material deforms at intermediate temperatures ($\sim$800C) by forming unstable shear bands, which flow via grain boundary sliding and cavitation. Al-though both strength and ductility increase with strain rate, polycrystalline strength decreases rapidly with increasing temperature.

Continuous SiC fiber-reinforced glass matrix composites have been tested in compression over a wide range in temperature and loading rate. Both uniaxial and crossplied fiber orientations were studied. Strength is found to depend sensitively on orientation and

(continued)

20. DISTRIBUTION/AVAILABILITY OF ABSTRACT	21. ABSTRACT SECURITY CLASSIFICATION
UNCLASSIFIED/UNLIMITED ☒ SAME AS RPT ☐ DTIC USERS ☐	Unclassified

22a. NAME OF RESPONSIBLE INDIVIDUAL	22b. TELEPHONE NUMBER (Include Area Code)	22c. OFFICE SYMBOL
James Lankford	512/522-2317	

DD FORM 1473, 83 APR   EDITION OF 1 JAN 73 IS OBSOLETE   UNCLASSIFIED

loading rate, while temperatures to 800C have less effect. Orientation effects are explained in terms of matrix microfracture and fiber buckling. The latter are shown to also control strengthening at very high (Hopkinson pressure bar) strain rates, where it is hypothesized that strength is enhanced by inertial effects which inhibit the development of the localized pockets of intense matrix microfracture and general buckling required for the nucleation of fiber kinks.

FOREWORD

This report describes recent work carried out under an experimental program aimed at characterizing damage mechanisms and compressive failure in ceramic-matrix composite materials. The report consists of two papers, each having been submitted to the journal noted on its title page.

Accession For	
NTIS GRA&I	☒
DTIC TAB	☐
Unannounced	☐
Justification	

By_____

Distribution/

Availability Codes

Dist	Avail and/or Special
A-1	

QUALITY INSPECTED 1

TABLE OF CONTENTS

TABLE OF CONTENTS (CONTINUED)

LIST OF ILLUSTRATIONS

LIST OF ILLUSTRATIONS (CONTINUED)

I.
DEFORMATION AND DAMAGE MECHANISMS
IN YTTRIA-STABILIZED ZIRCONIA

J. Lankford,* L. Rabenberg,** and R. A. Page*

Abstract

Yielding behavior and deformation modes are characterized for single crystal and polycrystalline yttria-stabilized ZrO_2 tested in compression from 23C to 800C. The plastic flow of single crystal specimens is orientation and temperature dependent, and is interpreted in terms of TEM evidence of dislocation activity, and an hypothesized tetragonal-to-cubic transformation. Polycrystalline material deforms at intermediate temperatures (~800C) by forming unstable shear bands, which flow via grain boundary sliding and cavitation. Although both strength and ductility increase with strain rate, polycrystalline strength decreases rapidly with increasing temperature.

*Department of Materials Sciences, Southwest Research Institute, San Antonio, TX.
**Department of Mechanical Engineering and Center for Materials Science and Engineering, University of Texas, Austin, TX.

INTRODUCTION

Zirconia-based ceramics stabilized with yttria to provide high volume fractions of the tetragonal phase have recently been shown to exhibit extremely attractive mechanical properties. For example, researchers have reported flexural strengths as high as 2 GPa,[1] and fracture toughness approaching 10 MPa $\sqrt{m}$.[2] Unfortunately, these results obtain only near room temperature; as the temperature is raised, both strength and toughness decline. This loss in toughness is generally attributed to diminution in the effectiveness of the tetragonal-to-monoclinic transformation as a source of inelastic strain. The latter can lead to toughening in a variety of distinct ways, as reviewed by Evans and Cannon.[1]

On the other hand, the very mechanisms of plasticity which enhance toughness in zirconia appear ultimately to be strength limiting.[3,4] In particular, the toughening mechanisms generally manifest themselves as microstructurally localized shear bands, produced by a cooperative precipitate transformation process documented most extensively for MgO-toughened PSZ. Chen and Morel[3] have recently shown that for the latter material, shear localization due to martensitic transformation plasticity is a principal source of microfracture, specifically at the intersections of shear bands and grain boundaries. These microfracture ensembles, rather than conventional intrinsic processing defects such as pores, are then responsible for failure via crack coalescence and/or growth.

Presently, the role of transformation plasticity in the development of damage in yttria-partially stabilized zirconia (Y-PSZ) has seen only limited study. This is despite the fact that some Y-PSZ systems exhibit

the extremely high strength/high toughness combination cited above and that phase transformations in Y-PSZ differ considerably from those in Mg-PSZ.[5] An experimental study of deformation and damage mechanisms in the Y-PSZ system is clearly desirable.

Moreover, current polycrystalline Y-PSZ is invariably characterized by a continuous amorphous grain boundary (GB) film, added during processing as both a sintering aid and as a means of limiting grain growth.[6] It is well known that in other glassy GB, but non-transformable, ceramic systems, elevated temperature mechanical properties are degraded by grain boundary sliding and creep cavitation within the glassy phase. This process has not yet been investigated for Y-PSZ.

A particularly effective means to evaluate the relative inelastic contributions of phase transformation versus grain boundary creep would appear to be to compare the deformation behavior of polycrystal and single crystal versions of nominally equivalent materials. Since single crystals of Y-PSZ are now available, this approach is feasible, and recent work has shown that the single crystal material has very interesting properties in its own right. While its low temperature toughness (9-10 MPa $\sqrt{m}$) is probably due to a reversible tetragonal to monoclinic transformation,[1] the even greater toughness (~15 MPa$\sqrt{m}$) at temperatures approaching 1500C must be caused by the extensive dislocation activity recently documented by Dominguez-Rodriguez, et al.[7,8]

The present report describes the results of a study of deformation, transformation plasticity, and related damage in single crystal and polycrystalline Y-PSZ. Particular attention will be directed toward behavior in the temperature range 700-800C; this is above the temperature for

effective tetragonal-monoclinic transformation toughening, but below that at which extensive dislocation activity has been observed.[7,8] Certain aspects of single crystal deformation are found to be common to those of polycrystals, and are invoked to explain the latter. On the other hand, it is observed that large scale yielding of single crystal and polycrystal variants can proceed along quite different paths.

EXPERIMENTAL PROCEDURES

Specimens for deformation experiments were fabricated from two types of yttria-stabilized ZrO_2. The first consisted of a large 5 wt.% Y_2O_3 zirconia single crystal,* which was oriented for sectioning using Laue X-ray diffraction. Cylindrical compression specimens 9 mm in length x 4.5 mm diameter were machined from the parent crystal, each having either a <123> or a <100> axial orientation relative to the cubic matrix. The microstructure of the as-received parent crystal contained a dense ($\gtrsim$ 50 volume percent) distribution of tetragonal precipitates; these precipitates are coherent with the matrix, commonly twin-related with each other, and in a variety of forms, ranging from distorted ellipsoids to parallel-epipeds. They are typically 400-1400 nm in length and 80-280 nm in width.

Crystals whose axis lay along <123> were oriented for single slip, with Schmid factors of ~0.45 for both {001}<011> and {111}<110> slip. The <100> crystals provided for multiple slip on either {111}[110] or {110}<110>, with Schmid factors of 0.408 and 0.5, respectively; slip on {001} planes was precluded.

_____

*Ceres Corp., Waltham, MA.

Polycrystalline specimens were machined from as-received sintered material in the heat-treated, partially stabilized condition.* Overall yttria content was roughly the same (5.8 wt.%) as for the single crystals, but it has been shown[6] that for the two ZrO_2 phases present, the Y_2O_3 concentrations differ significantly. In particular, the preponderance of the grains were ~0.5 μm diameter tetragonal phase, with an yttria composition of 3.0-4.1 wt.%. The remainder of the material was composed of occasional Al_2O_3 grains, and cubic zirconia grains on the order of 0.6-2.0 μm in diameter, with a Y_2O_3 composition of 6.7-9.4 wt.%. All grain boundaries are covered by a ≤10 nm thick amorphous grain boundary phase, composed of Y_2O_3, SiO_2, Al_2O_3, and possibly ZrO_2.

Ambient material properties for both materials studied are presented in Table I. Also included for comparative purposes are equivalent properties of an MgO-stabilized polycrystalline PSZ.** It should be noted that available evidence indicates[9] that MgO-PSZ also possesses an amorphous GB film.

Specimens were tested at temperatures ranging from 23C to 800C, and at strain rates of $10^{-5}s^{-1}$ to $10^{-1}s^{-1}$. For elevated temperature testing, specimens were allowed to soak for thirty minutes in order to ensure that they were at equilibrium; it has been shown[10] that this period is insufficient to cause measurable loss of strength. Experiments required the use of ceramic loading platens, which were fabricated from high strength alumina; both specimens and platens were ground and lapped parallel to

---

*Norton YZ 110 TZP; Norton Company, Northborough, MA.

**Nilsen TS-Grade PSZ; Nilsen Sintered Products, Ltd, Northcote, Vic, Australia.

TABLE I

MATERIAL PROPERTIES

Material	Flexural Strength (MPa)	Hardness (GPa)	Fracture Toughness (MPa√m)	Grain Size (μm)
Y-PSZ Single Crystal	1384	13.6	6.9	–
Y-PSZ Polycrystal	1000	13.0	8.5	0.5-2.0
Mg-PSZ Polycrystal	600	10.2	8-15	60

within 2 μm. Smooth (0.05 μm diamond) flats were polished onto certain specimens, to provide evidence of damage produced during testing; the latter was characterized by Nomarski microscopy and scanning electron microscopy (SEM), and transmission electron microscopy (TEM) of two-stage carbon surface replicas. Specimens for thin foil TEM were then sectioned, dimpled, and ion milled. Sectioning was performed both normal to the compression axis, and parallel to observed slip planes.

RESULTS

Stress-Strain Behavior

In Figure 1, stress (σ) is plotted versus axial strain (ϵ) for polycrystalline Y-PSZ tested at a strain rate ($\dot{\epsilon}$) of $10^{-5}s^{-1}$; included for comparison are recent data[11] for the Mg-PSZ described in Table I. Both yield and ultimate strength are very temperature sensitive for Y-PSZ, whereas for the Mg-stabilized material both parameters are temperature insensitive. Regardless of stabilizer chemistry, ductility increases with temperature.

It is interesting to note that the flow stress curves for the Y-PSZ are smooth and continuous, while the yielding of Mg-PSZ is jerky, or serrated. Furthermore, following initial yield, Y-PSZ specimens tested at 400C and 800C suffered load drops, the amplitude of which decreased with increasing temperature. No such drops were observed for Mg-PSZ.

The σ-ϵ behavior of Y-PSZ single crystals was very sensitive to crystal orientation and temperature. For crystals oriented along <123> (Figure 2a), yielding at 23C took place at a high stress level (nearly 3 GPa), followed by monotonic hardening to an ultimate plastic strain
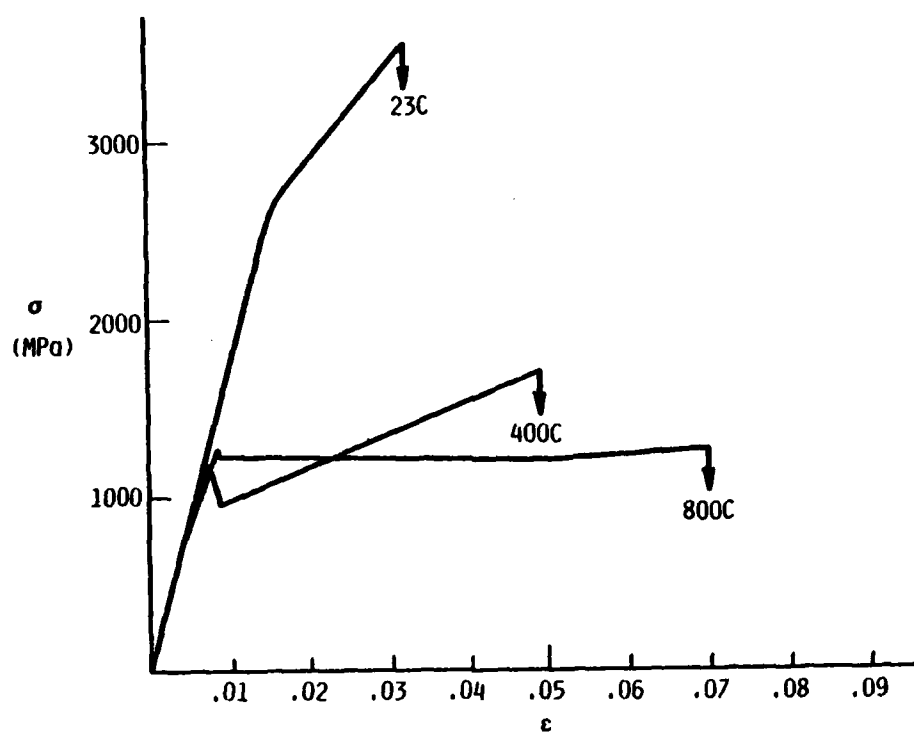
(a) Y-PSZ
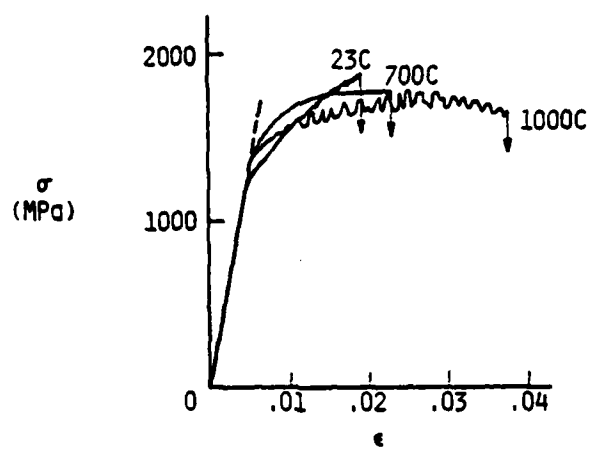
(b) Mg-PSZ

Figure 1. Stress-strain for polycrystalline ZrO_2, $\dot{\epsilon} = 10^{-5}s^{-1}$.

of ~0.005. At higher temperatures, yield and ultimate strengths were drastically reduced, while strain to failure increased to ~0.06 for T = 700C. This deformation was realized via a non-hardening, extremely erratic flow process.

Crystals oriented along <100> behaved in a remarkably different fashion; as shown in Figure 2b, yielding occurred in two stages. First, at a temperature-dependent stress level during elastic loading, the specimen instantaneously deformed to a plastic strain of 0.0049, at which point elastic deformation resumed. For ambient conditions, the specimen then broke in a brittle mode. At 700C, on the other hand, specimens yielded via a load drop, followed by smooth, monotonic hardening to an ultimate plastic strain in excess of 0.15.

Yielding was also found to exhibit strain rate sensitivity, an effect most evident at elevated temperatures (Figure 3). As shown in Figure 3a, the <100> single crystal pre-yield incremental strain plateau again represents a plastic strain of 0.0049, but the stress level at which this occurs is significantly higher with increasing $\dot{\varepsilon}$. Moreover, the macroyield stress, the amplitude of the load drop, and the ultimate strength all are greater at the higher loading rate, while the ductility is significantly reduced. Crystals oriented along <123> also increased in yield and ultimate strength, and decreased in ductility, with increasing strain rate; however, yielding was never preceded by a load drop.

The strain rate dependence of polycrystalline deformation (Figure 3b) was similar to that of the <100> single crystals in some respects, but different in one important regard. Again, the zirconia yields prior to the load drop, but this time the rate-dependent yielding takes place over

(a) <123> orientation

(b) <100> orientation
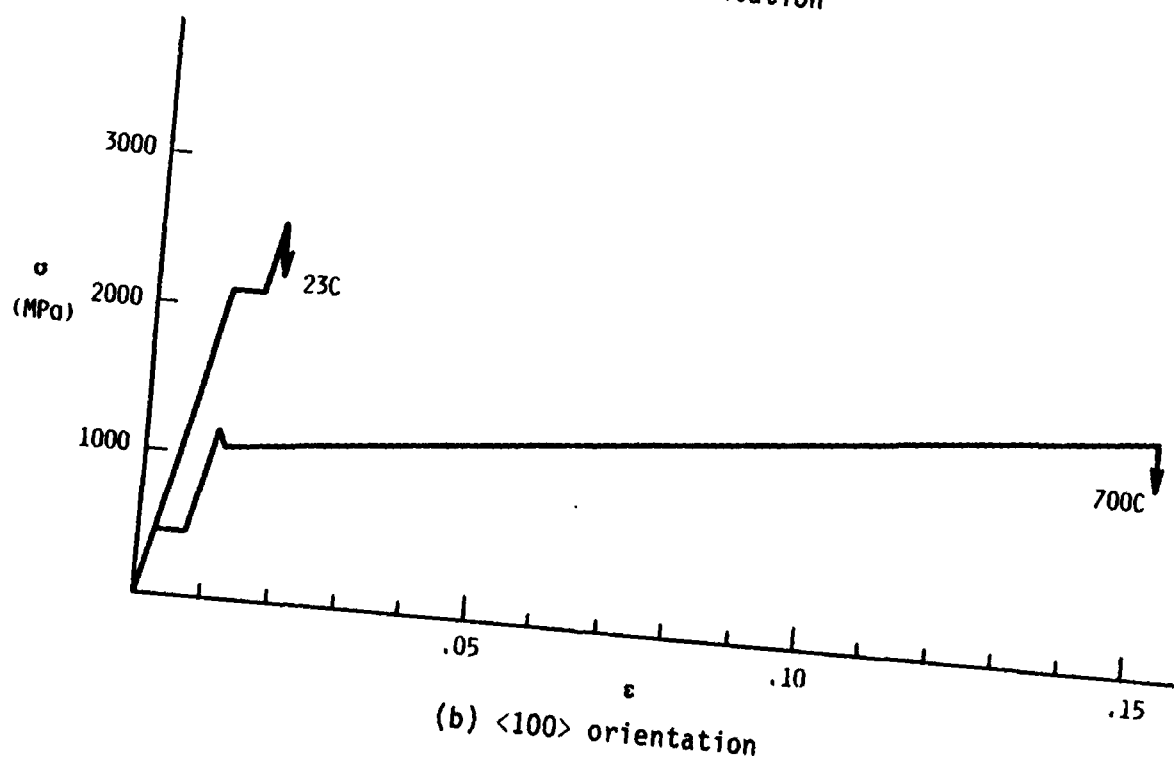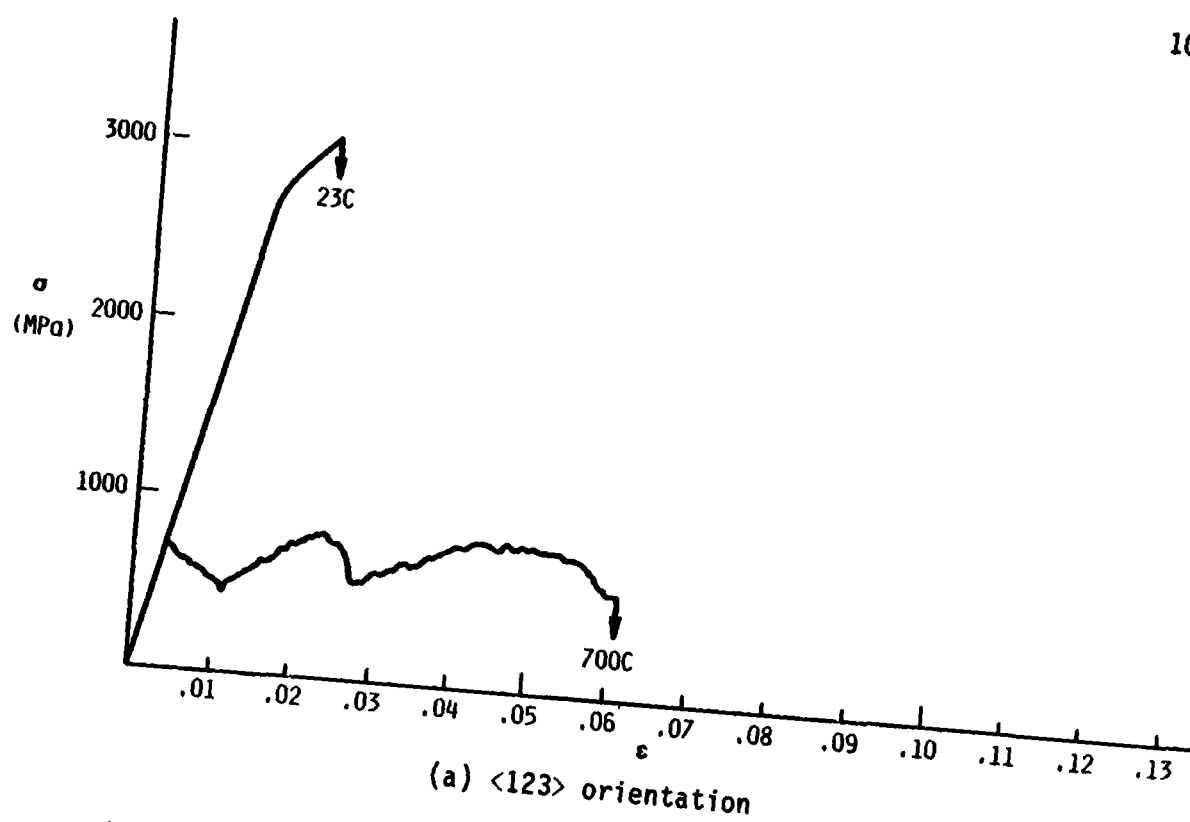
Figure 2. Stress-strain for Y-PSZ single crystals, $\dot{\epsilon} = 10^{-5}s^{-1}$.
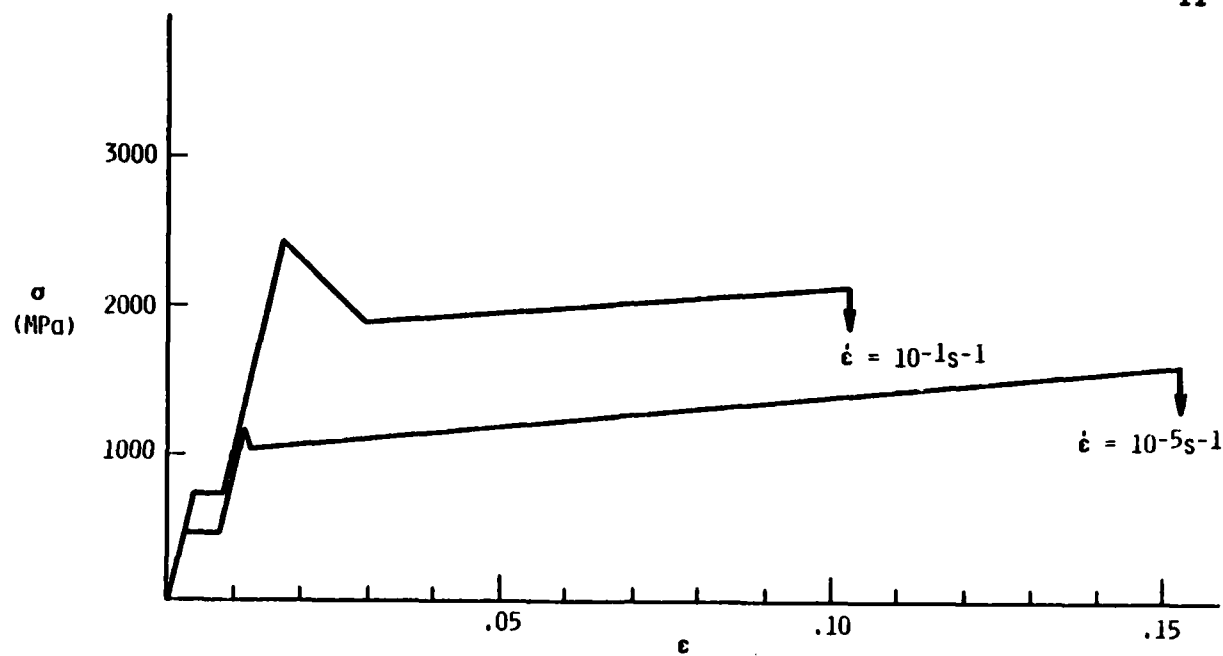
(a) Y-PSZ,<100>, T = 700C
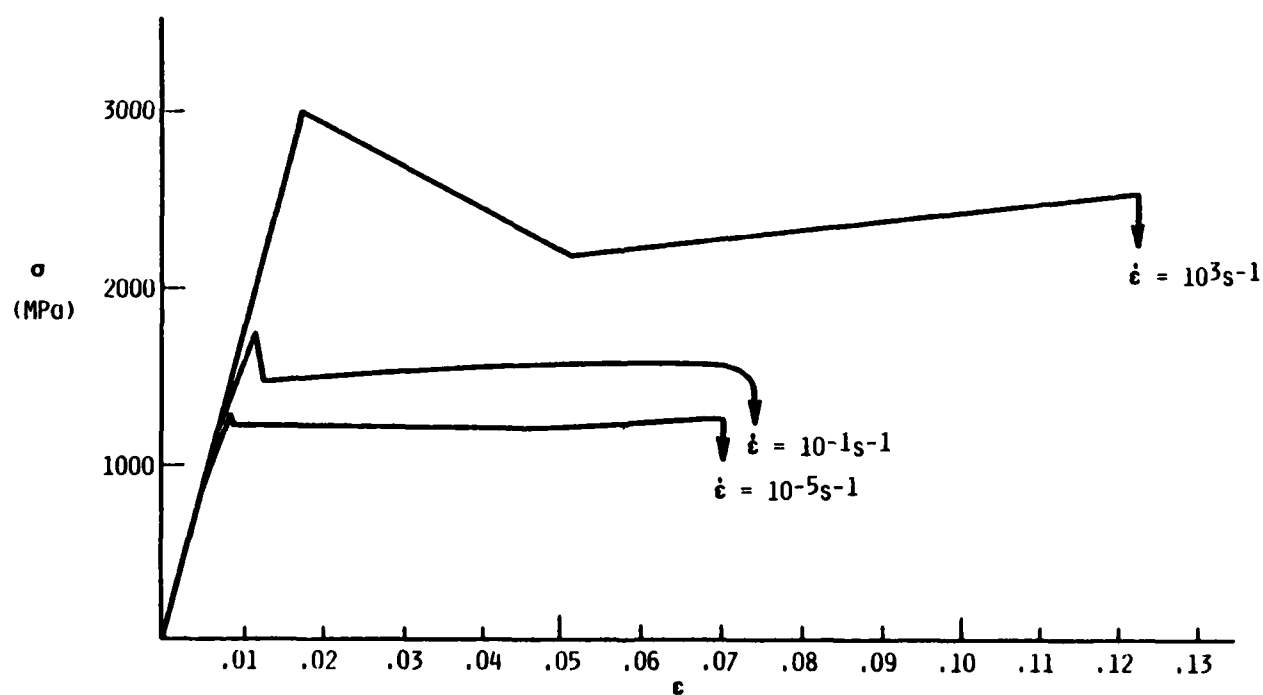
(b) Y-PSZ Polycrystal, T = 800C

Figure 3. Stress-strain for Y-PSZ tested at varying strain rate.

a range of stresses, so that deformation occurs gradually, rather than in a single burst. As for the single crystals, the macroyield point, the amplitude of the load drop, and the ultimate strength increase with strain rate. However, it is surprising to note that as $\dot{\varepsilon}$ increases from $10^{-5}s^{-1}$ to $10^{-1}s^{-1}$, there seems to be an _increase_ in ductility. In order to evaluate whether this is indeed a real and significant effect, a few tests were performed at 800C in a Hopkinson pressure bar (HPB) facility, yielding stress-strain data for $\dot{\varepsilon} = 10^3s^{-1}$. A typical result is shown in Figure 3b, where it is abundantly evident that by loading at this extremely high rate, both the strength and ductility of the ceramic have been greatly enhanced.

The foregoing results raise a number of questions, including the following: (1) Why is the strength of polycrystalline Y-PSZ more temperature sensitive than that of Mg-PSZ? (2) What is the origin of the approximately 10% ductility observed for <100> single crystal and polycrystalline Y-PSZ in the relatively low temperature range of 700-800C? (3) Why do <123> single crystals flow in a jerky fashion, while <100> specimens harden monotonically? (4) What is the origin of the gradual yielding which precedes the polycrystalline Y-PSZ upper yield point? (5) What is the origin of the pre-macroyield plastic "step" observed for the <100> single crystals?

Deformation and Damage Mechanisms

In order to obtain some idea of the origin of the <100> single crystal preyield plastic "step", specimens with a polished flat were unloaded immediately following "steps" at both 23C and 700C. Optical inspection revealed no evidence of deformation, but examination of TEM

replicas showed (Figure 4) extensive transformation of platelike precipitates oriented with their axes (minimum dimension) parallel to the compressive stress axis.

At elevated temperatures (250 $\lesssim$ T $\lesssim$ 700C) the onset of macroscopic yielding for single crystals of both orientations corresponded to the initiation of Luders bands. In the case of the <123> specimens, slip began at one end of the specimen, and propagated throughout the volume by means of planar slip on {001}<011> (Figure 5a). Specimens ultimately failed by crack nucleation and slip-off on {001} planes. For similarly oriented crystals, this same slip system was observed for Y-PSZ (8-32 wt.% Y_2O_3)[7,8] and for Ca-PSZ,[12] tested in compression at T $\cong$ 1400C.

Specimens of <100> orientation also yielded via a Luders process, but it was considerably more complex than that observed in the preceding case. The initiation of the flow process corresponded to the nucleation of intersecting slip bands, which began to propagate down the specimen as deformation proceeded. Shortly afterward, a second Luders process began, which followed along about a millimeter behind the dislocation front. This second front produced marked surface rumpling, and appeared to be caused by precipitate transformation; an example of a region traversed by both fronts is shown in Figure 5b. X-ray diffraction indicates that the trace of the slip planes is {110}, suggesting {110}<110> slip. This is contrary to the results of Dominguez-Rodriguez, et al[7] for 16.9 wt.% Y-PSZ oriented 4° from <100> and tested at 1400C, in which case deformation occurred on {111}<110>.
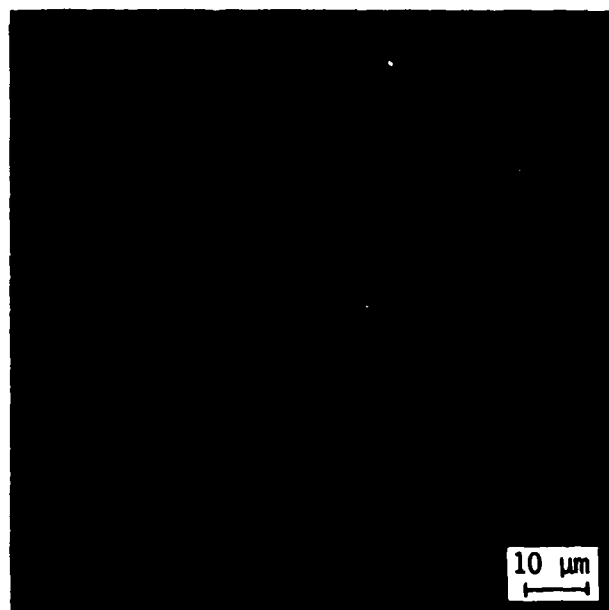
Figure 4. Precipitate transformation during <100> single
crystal preyield plastic "step" at T = 23C.
Stress axis is roughly vertical.
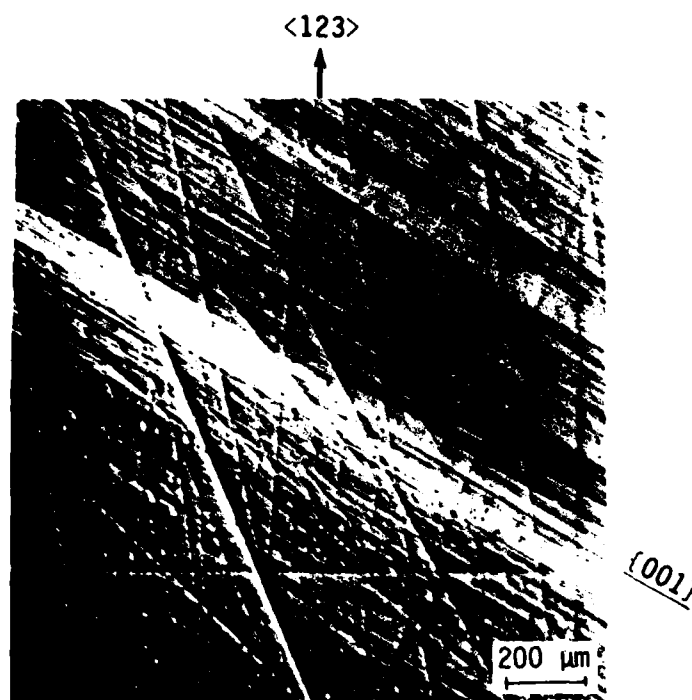
(a) <123> orientation, ε = 0.015,
showing planar slip bands.
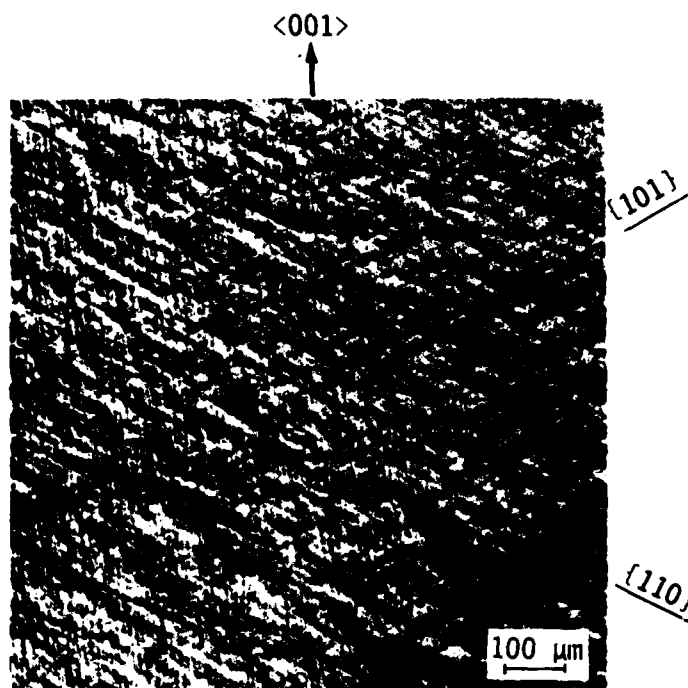
(b) <100> orientation, ε = 0.03, showing
multiple slip and surface rumpling
caused by precipitate transformation.

Figure 5. Nomarski contrast evidence of single crystal
Y-PSZ deformation at T = 700C, $\dot{\varepsilon}$ = $10^{-5}s^{-1}$.

Transmission electron microscopy of deformed specimens was difficult, due to distortion caused by both transformation-induced strains and by dislocations. At 700C, the original microstructure is almost unrecognizable (Figure 6), and many domains are faulted. Extended partial dislocations appear to lie on certain faults (arrows, Figure 6). Individual dislocations were occasionally observed at combined strains and temperatures as low as 0.005 and 283C, respectively.

For the multiple slip <100> orientation, two general types of deformation features are evident. Figure 7a-b shows a very high density of dislocations lying within complex dislocation cell walls. The defect density is so high that it is very difficult to image individual dislocations. Many segments seem to be present, as evidence of extensive mutual cutting of dislocation on several systems. Other regions exhibit large populations of transformed precipitates (Figure 7c-d). Of particular interest are the numerous microscopic cracks present throughout (arrows), some of which exceed barely 40 nm in length. Microcracks were associated only with transformed particles, usually spanned the minimum precipitate dimension, and were never observed within the dislocation tangles or cells.

At room temperature, the <100> crystals failed in a brittle mode, while the <123> specimens deformed slightly (Figure 2) prior to failure. However, the latter displayed no slip line evidence of dislocation activity, and Raman microprobe analysis detected no monoclinic phase in a yielded but unfailed crystal.

Figure 6. TEM of <123> crystal, T = 700C,
ε = 0.015. Foil is normal to
<123>.
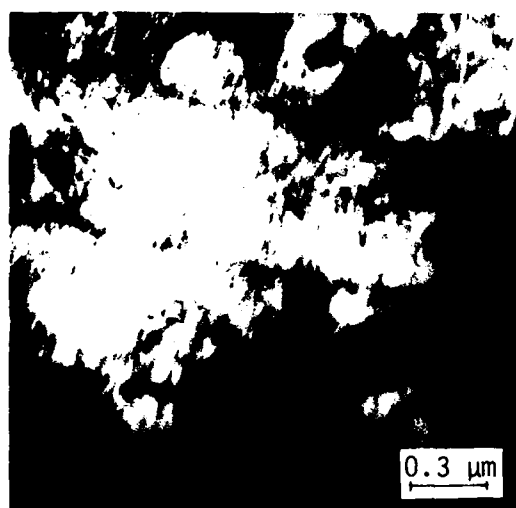
(a) Dislocation tangles and cell walls.
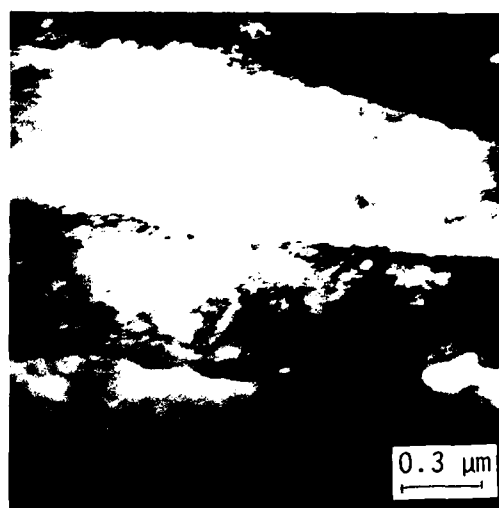
(b) Tilted view of (a).
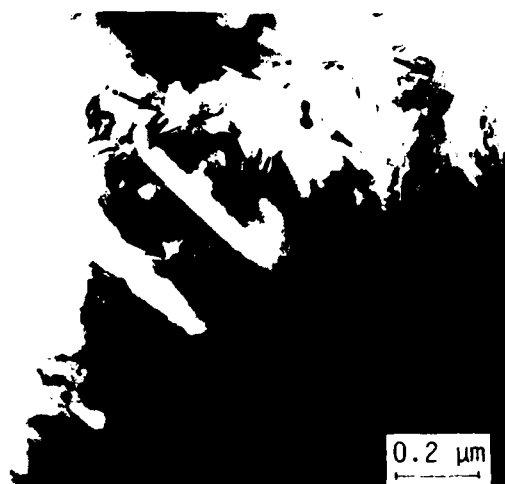
(c) Transformed particles, and associated microcracks (arrows).

(d) Transformed particles, and associated microcracks (arrows).

Figure 7. TEM of <100> crystal, T = 700C, ε = 0.03. Foil is normal to <100>.

These single crystal deformation mechanisms invite both comparison and contrast with those characteristic of Y-PSZ polycrystals. For example, the gradual deformation of polycrystalline specimens which preceded their macroyield load drop at all temperatures was accompanied by extensive, homogeneous transformation (Figure 8). The possible relationship between this yield behavior, and the single crystal pre-yield incremental strain step, will be developed later.

The bulk yielding process, on the other hand, was amply visible, and is shown in Figure 9 for a specimen tested at 800C. Again specimens yielded through the nucleation and propagation of a Luders front, but here (Figure 9a) it is one which produces inhomogeneous, intersecting shear bands. Closer inspection shows that the bands have rather a dimpled appearance (Figure 9b), evidence no dislocation slip, and are separated by blocks of apparently undeformed material. The bands are oriented at an average angle of 45° relative to the compressive stress axis.

Transmission replica microscopy (Figure 10a) shows that the deformation bands are actually regions in which high shear strains are accommodated by grain boundary sliding, with attendant formation of intergranular, axial microcracks. Upon close inspection of the figure, it can be seen that within the shear bands, grain boundaries are generally visible, whereas they are invisible in the relatively undeformed blocks adjacent. The basis for this effect can be seen in Figure 10b-c, where it is evident that the grain boundaries are decorated by small, roughly spherical, cavities which have nucleated on certain facets and, frequently, coalesced to form grain-sized microcracks. The latter can then coalesce to form larger, multigrain size cracks, especially where shear
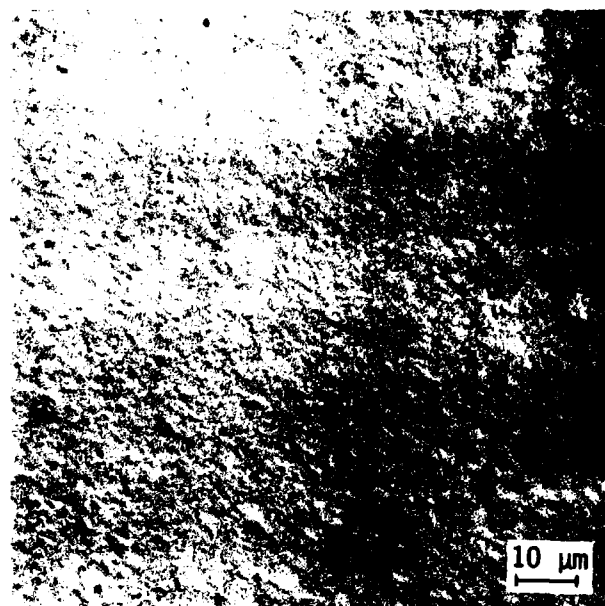
Figure 8. Nomarski contrast view of surface rumpling caused by transformation of polycrystalline Y-PSZ deformed within preyield region, T = 23C, $\dot{\epsilon} = 10^{-5}s^{-1}$. Stress axis is vertical.
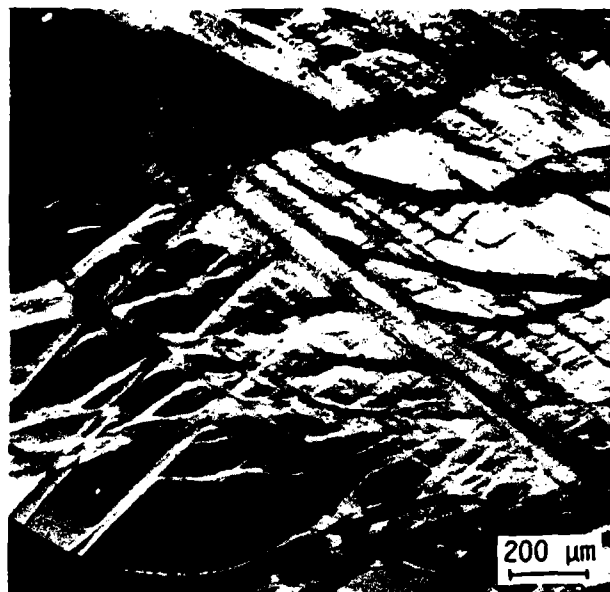
(a) Deformation in wake of Luders front, showing inhomogeneous shear bands.

(b) Higher magnification of typical deformation band, showing fine scale rumpling, and no slip lines.

Figure 9. Nomarski contrast view of polycrystalline Y-PSZ deformed to $\epsilon = 0.05$ at $T = 800C$, $\dot{\epsilon} = 10^{-5}s^{-1}$. Stress axis was vertical.
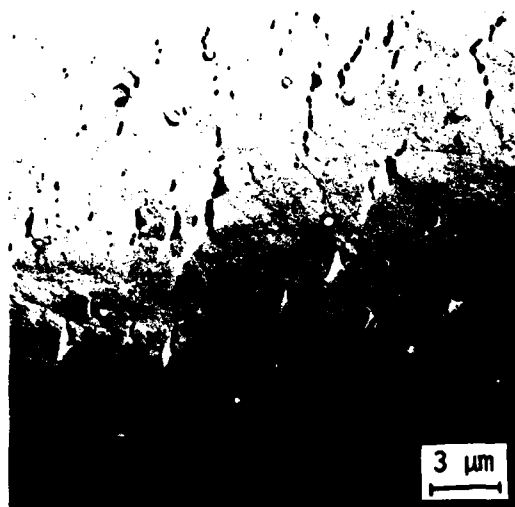
(a) Deformation band with axial intergranular
cracks and visible grain boundaries.
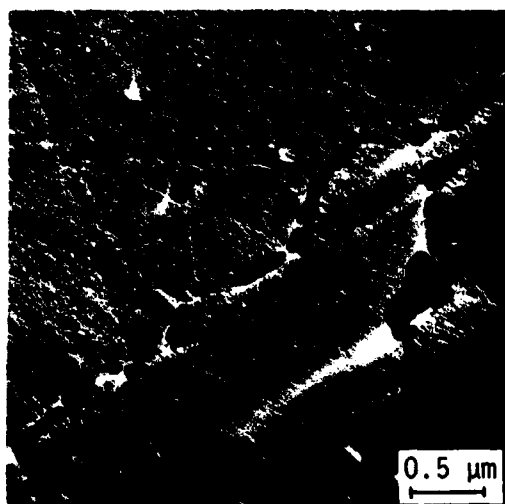
(b) Multiple-cavitated grain
boundary facets.
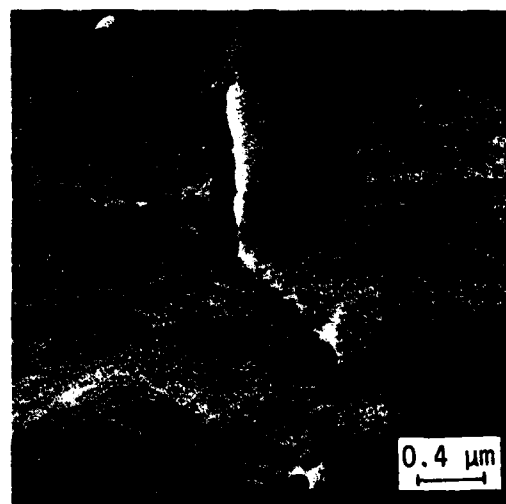
(c) Formation of axial grain
boundary microcrack via
cavity coalescence.

Figure 10. TEM replica of deformation shear bands in polycrystalline Y-PSZ,
$\varepsilon = 0.05$, T = 800C, $\dot{\varepsilon} = 10^{-5}s^{-1}$. Stress axis is vertical.

bands intersect (Figure 11). Such sites become the origins of localized failure (Figure 12a), i.e., regions of gross intergranular separation (Figure 12c) created by high local shear strains (Figure 12b).

The situation just described is complicated by other factors. Prior to deformation, grain boundaries are smooth, and grain interiors are relatively free of defects (Figure 13a). During initial yielding, transformation of tetragonal phase occurs (Figure 13b), as manifested in the surface relief described earlier (Figure 8). However, as deformation proceeds, originally smooth grain boundaries begin to assume a wavy profile (arrows, Figure 13c). The "waves" often seem to be associated with local transformed regions. At other locations, cusps develop at the intersections of transformed layers and grain boundaries (arrow, Figure 13d). The possible significance of these features will be discussed in the following section.

DISCUSSION

One of the most interesting experimental observations was the unusual incremental strain "step" which preceded macroscopic yielding/failure in the <100> single crystal specimens. Recalling that the activation stress for the "step" is temperature and strain rate sensitive, that the strain burst amplitude was constant at 0.0049, and that transformed precipitates were observed immediately following, it seems reasonable to suspect a thermally activated transformation as the origin.

Two possibilities can be envisaged, one involving the familiar tetragonal-to-monoclinic ($t \rightarrow m$) phase change, the other a tetragonal-to-cubic ($t \rightarrow c$) reversion. In the case of the $t \rightarrow m$ transformation, it at first seems unlikely that this could account for a thermally activated process,

20 µm
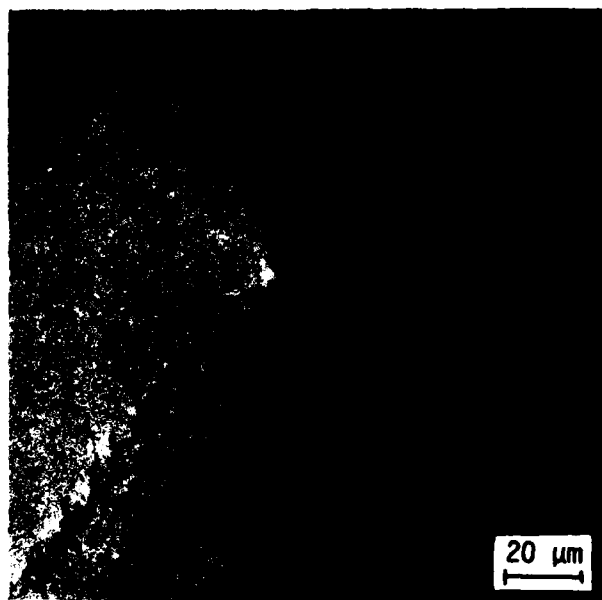
Figure 11. Microcrack formation at intersection of shear bands. Stress axis is vertical, ϵ = 0.05, T = 800C, $\dot{\epsilon}$ = $10^{-5}s^{-1}$.

(a) Localized damage (arrow) at intersection of shear bands.

(b) Higher magnification view of (a), showing intense local shear deformation.
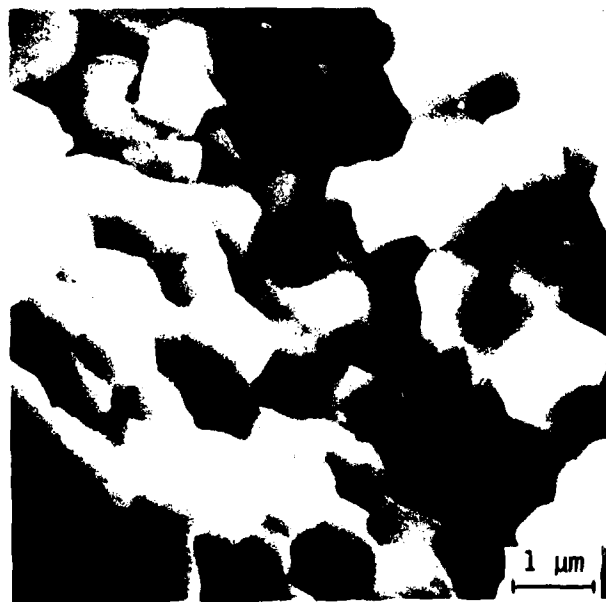
(c) Higher magnification view of (b), showing intergranular separation.

Figure 12. Localized intergranular failure at site of shear band intersection. $\varepsilon = 0.05$, $T = 800C$, $\dot{\varepsilon} = 10^{-5}s^{-1}$. Stress axis is vertical.

(a) Undeformed microstructure.
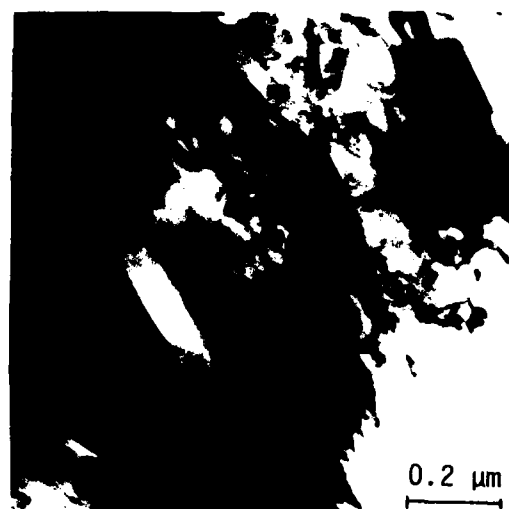
(b) Deformation-induced tetragonal to monoclinic transformation.

(c) Deformation-induced grain boundary waviness (arrow).
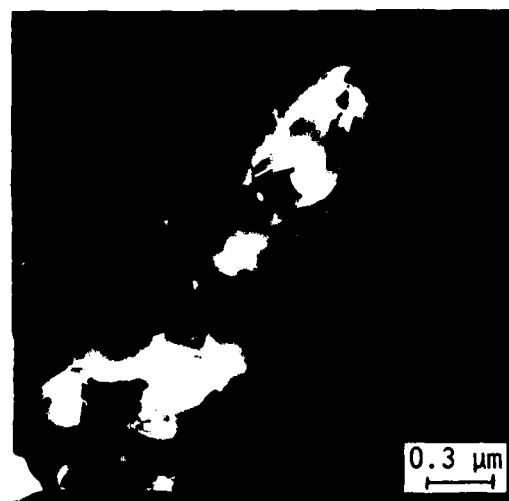
(d) Transformation-induced grain boundary cusps (arrow).

Figure 13. Transmission electron microscopy of polycrystalline Y-PSZ specimen deformed to a strain of 0.05 at T = 800C, $\dot{\epsilon}$ = $10^{-5}s^{-1}$, compared with undeformed microstructure.

since it is well known[1] that the transformation is martensitic. However, Ruhle, Claussen, and Heuer[6] have recently observed the dynamics of the t→m transformation in polycrystalline Y-PSZ, and found that it can be remarkably sluggish. Regions of reduced Y_2O_3 content corresponded to increased likelihood of nucleation, and increased speed of transformation. In the case of the present single crystals, yttria content is uniform in the tetragonal particles, so that all of a given orientation would be expected to transform at the same stress level; the latter would depend upon the specific combination of temperature and loading rate.

The data support the alternative possibility of a t→c transformation; this can be rationalized as follows. The tetragonal particles are believed to form from the cubic by a composition-invariant, displacive transformation,[5,13] and since they are believed to assume a morphology which minimized strain energy, the imposition of an external stress is expected to shift the balance and promote growth or shrinkage of a given tetragonal particle at the expense of another, or of the cubic phase, if present. As these tetragonal particles have a higher than equilibrium yttria content, and are coherent with the matrix, they are very reluctant to transform to monoclinic. Furthermore, the tetragonal to monoclinic transformation would require a significant volume expansion against the compressive stress. Instead, the t→c transformation occurs to accommodate the applied stress. The t→c reversion should occur more easily at elevated temperature where the free energy difference between the cubic and tetragonal phases is expected to be smaller. Thermal activation is expected to play a role in this process, since reversion would be accomplished by simultaneous alteration of the tetragonal c-axis dimension and

slight shifting of the oxygen ions. The latter process would be accomplished by thermally activated jumps under the influence of an applied compressive stress along the c-axis.

For this scenario to be feasible, it must at least be compatible with the present single crystal results. Within the <100> single crystals, three t-precipitate variants were present, two sets with their c-axes normal to the compressive stress axis, and one set with its c-axes parallel to it. If these precipitates reverted to cubic with some attendant shape change, they would be expected to have the appearance of the precipitates in Figure 4. This would imply that the compressive stress components in the c-direction which were required to activate the reversion at $\dot{\varepsilon} = 10^{-5}s^{-1}$ and T = 23C and 700C were (from Figure 2b), ~2100 MPa and ~450 MPa, respectively.

Taking into account the orientation of the most favorably oriented tetragonal variants in the <123> crystals, axial stresses of approximately 3300 MPa and 700 MPa would be needed in order to produce the t-c reaction. Recalling Figure 2a, gradual yielding at 23C began at 2600 MPa, and failure occurred below 3100 MPa, while at 700C serrated yielding began on (100) planes at a stress of approximately 700 MPa. Based on the idea of a critical stress for t→c transformation, it is not surprising that a strain burst was not observed at 23C, but one would have been expected at the higher temperature.

However, it should be noted that compressive loading of the <123> crystal provides not only a compressive stress component along tetragonal c-axes, but also a significant shear component along [$\overline{1}\overline{1}0$](001). While the compressive stress provides a driving force for transformation, its

shear component also could drive dislocations on the observed slip system. Since tetragonal particles are elongated normal to their c-axis as sketched in Figure 14a, reorientation probably will require nucleation of misfit dislocation loops of [$\bar{1}$00] Burgers vector (Figure 14b). These loops would dissociate into [$\bar{1}$10] and [$\bar{1}\bar{1}$0] segments, and the applied stress would tend to drive the [$\bar{1}\bar{1}$0](001) segments through the crystal. Such a process might account for behavior of the <123> crystals at 700C; once the applied stress nears 700 MPa, the t-c transformation occurs within the most highly stressed region of the specimen. Before other precipitates can transform, the stress is relaxed by the avalanching of misfit dislocations through the crystal, creating an autocatalytic Luders process. The specimen finally fails in shear by sliding off when the single slip system is exhausted, and slip band cracks nucleate.

In the case of <100> crystals, on the other hand, the resolved shear stress on the misfit dislocation (001) slip planes is essentially zero, hence, as expected, no deformation takes place immediately following the preyield "step". Instead, slip is finally activated on the next most favored system, {110}<110>. It was noted that Dominguez-Rodriguez, et al,[7] observed {111}<110> slip in near (4°) <100> crystals. However, the temperature was much higher than in the present case (1400C versus 700C). Furthermore, the tetragonal precipitate microstructure was unavoidably different, due to the yttria content (16.9 wt.% versus 5%). Finally, the
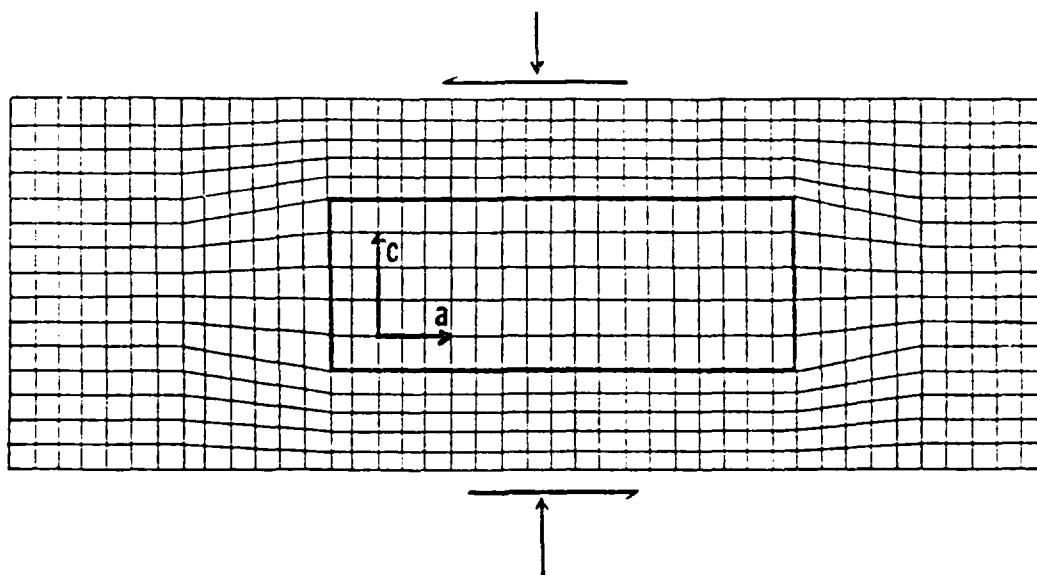
Figure 14a. Schematic sketch of a two-dimensional section through one of the t'-ZrO$_2$ plates within the c-ZrO$_2$ crystal. For the ⟨100⟩ stress axis orientation, a normal and a shear component of stress exist on the face of the t' plate. The degree of tetragonality and the elastic strains are highly exaggerated.
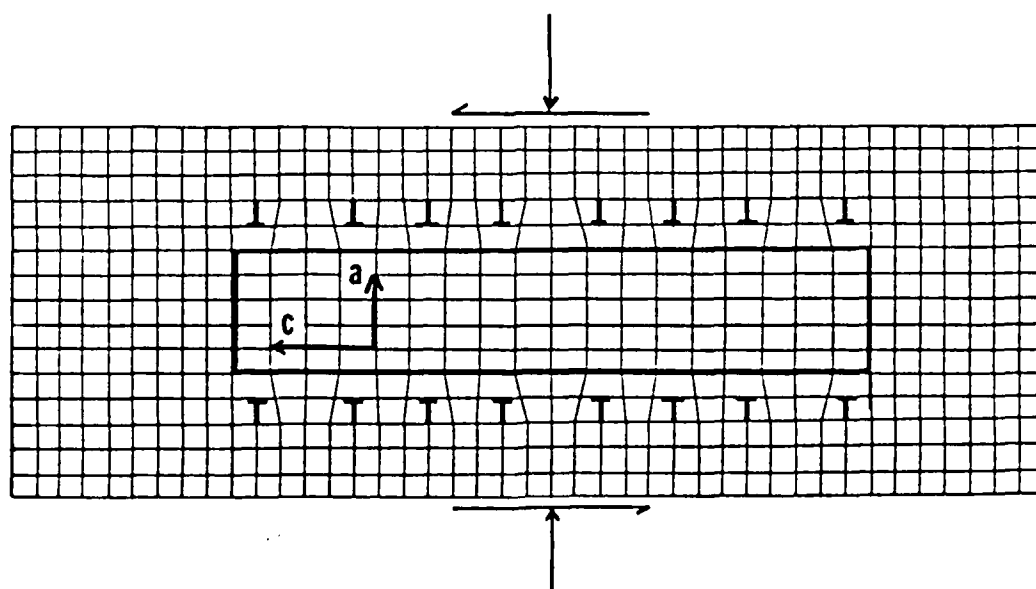
Figure 14b. Schematic sketch of a t'-ZrO$_2$ plate in a cubic matrix after reorientation of the c-axis under an applied stress. Misfit dislocations of b = [100]$_c$ are required by geometry.

Schmid factor for {111}<110> slip was 0.47 in the work of Dominguez-Rodriguez, compared with the present 0.408; in both cases, the Schmid factor for {110}<110> slip was 0.5. Based on these significant differences, and the greater disparity in resolved shear stress on the competing slip systems, the results obtained seem reasonable.

Since multiple planes are involved, due to the loading symmetry, flow is stable and hardening. It is this stable dislocation flow which accounts for the remarkably high ductility of <100> versus <123> crystals. Furthermore, since a transformation Luders front follows the initial multislip front through the crystal, it is possible that the apparent t→m transformations were nucleated by the local stresses at dislocation pile-ups, etc. The specimen apparently failed by the coalescence of the transformation-nucleated microcracks; thus, its demise was ultimately related to the deformation which, for a period, had extended its life.

It will be recalled that Y-PSZ polycrystals yielded gradually, before either failing (at 23C) or experiencing a load drop followed by macroscopic strain (T ≳ 400C). Further, surface rumpling caused by transformations was observed within this early flow regime. Grains within the sample were randomly oriented, so that c-axes were likewise randomly distributed relative to the load axis. That being the case, crystallites less favorably oriented for t→c transformation would require higher axial stresses in order to transform. This distribution in activation stress would lead to the rapidly hardening early stage of yielding shown in Figure 1a.

However, the macroscopic yielding of the polycrystalline ZrO_2 is not at all comparable with the dislocation mechanisms responsible for flow in single crystals. This is not surprising, considering the inverse strain rate effect shown in Figure 3. The behavior of the <100> single crystal (Figure 3a) represents a classic example of the suppression of dislocation motion (decreased ductility), and a corresponding increase in strength, with increasing strain rate. The polycrystalline material, on the other hand, is not only strengthened, but its ductility is enhanced as well, with more rapid loading (Figure 3b). This curious and possibly unique effect is probably due either to delay in the onset of instability represented by nucleation of the creeping shear bands themselves, or to retardation of the cavitation process responsible for shear band failure. It is very interesting to note that the energy of failure at $\dot{\epsilon} = 10^3 s^{-1}$ calculated on the basis of the area under the stress-strain curve, is nearly four times that obtained for $\dot{\epsilon} = 10^{-5} s^{-1}$.

The formation and evolution of the compressive shear bands affords an interesting comparison, and some contrast, with the recent work by Dalgleish et al,[14,15] on creep rupture during bending of polycrystalline alumina. For the latter relatively fine-grained (4 μm) material, characterized by a glassy grain boundary phase, failure in the absence of large pre-existing flaws was caused by the coalescence of facet-sized, shear band microcracks. The microcracks nucleated via cavitation and cavity linkup on planes normal to the tensile axis, and congregated into shear bands whose normal projections were, on average, about 60° from the stress

axis. Many bands were observed[14] to initiate at microstructural or chemi-
cal heterogeneities. Testing was performed at constant stress at tempera-
tures $\geq$ 1250C, with shear band formation occurring only for specimens
which failed via creep damage coalescence at strains in excess of 0.08.
At smaller strains, failure occurred by the growth of a single dominant
crack nucleated at an inherent processing flaw. Shear banding was not
observed on the compressive sides of the failed bend specimens.

Testing of the present ZrO_2 material was performed at constant
strain rate, although once the material began to flow at 800C, the stress
remained essentially constant (Figure 1a). Deformation development dif-
fered markedly from that observed for the Al_2O_3 tested in bending,[14,15] in
that shear bands (which again corresponded to large failure strains,
i.e., $\epsilon_f \simeq 0.07$) were observed in compression. However, it is likely that
the alumina[14,15] simply failed in tension before the compressive stress
reached the level required for the nucleation of compressive shear bands.

As for the Al_2O_3, cavitation and microcrack nucleation (cavity
coalescence) in the zirconia took place on grain boundaries approximately
normal to local tensile stresses, i.e., on facets containing the compres-
sion axis. However, the shear bands within which these processes occurred
did not lie at 30° to the principal stress axis, as they did for tensile
loading of alumina.[14,15] Instead, the bands were oriented roughly 45° to
the stress axis, and they never seemed to be associated with material
flaws. This suggests that the damage localization manifested in the bands
probably derived from an instability in the macroscopic homogeneity of
deformation.

This sort of situation has been analyzed theoretically by Rudnicki and Rice[16] for the case of multiple microfracture of brittle materials, leading to shear faulting. The present case is different, to the extent that the "pre-existing flaws" are not randomly oriented fissures, but rather are inclined grain boundaries which at elevated temperature may slide to permit cavitation on adjacent boundaries containing the compressive load axis. The sliding boundaries are thus "lubricated" by the viscous GB phase, a factor not included in the treatment of Rudnicki and Rice.[16] Nevertheless, the latter indicates that for reasonably low coefficients of sliding friction, such as might obtain in the present case, the inclination of shear bands relative to the stress axis is dominated by dilatation. Extensive cavitation and associated multigrain macrocracks produce high dilatation, as obtained in the tensile experiments of Dalgleish, et al.[14,15] The pertinent deformation localization analysis[16] predicts an angle of shear band inclination of ~60°, as observed experimentally.[15]

In the present zirconia compression experiments, it is evident that shear band dilatation is low. The predominant damage features seem to be isolated cavities, and widely dispersed, facet-sized microcracks. Under such circumstances, the theoretically predicted[16] shear band angle of incidence would be ~45°. This prediction is borne out experimentally (Figure 9a).

The observed cavitation mode, in which multiple, more-or-less equal-sized cavities seem to form on a GB facet (Figure 10 b-c), is similar to the stochastic process established via small angle neutron scattering[17] for hot-pressed (glassy GB) SiC. In this case, involving compressive

creep at much higher temperature (1600C), the material deformed homogeneously without forming shear bands.

Finally, the Y-PSZ shear bands appear to represent localized superplastic flow. It is the absence of these zones of intense shear which differentiates this material from the large-grained Mg-PSZ whose behavior was cited in Figure 1(b). Although some grain boundary sliding may occur in the latter material, the 60 μm grains are too large to permit superplasticity, which generally requires grain dimensions on the order of a few micrometers or less. Only in such cases is it possible for diffusive (or viscous, in the present case) grain boundary flow to dominate intragranular power law (plastic) creep, and to permit strain rate-sensitive grain boundary sliding to control material deformation. Under such circumstances, superplastic deformation of ceramics with viscous GB films can be achieved.[18]

CONCLUDING REMARKS

It is evident that for both single crystal and polycrystalline Y-PSZ, failure is governed by the development of shear instabilities. The latter are an inevitable consequence of the deformation mechanisms (martensitic and/or thermally activated transformations, dislocation activity, grain boundary sliding/cavitation) which impart higher toughness to this class of ceramic alloy. It is interesting to observe that the materials resemble metals, to the extent that they do in fact deform, and that their uniaxial compressive-to-tensile strength ratio is much lower than that usually found for ceramics, i.e., $8 \gtrsim \sigma_c/\sigma_T \gtrsim 20$. For metals, $\sigma_c/\sigma_T \simeq 1$, which is essentially the case for single crystal and polycrystal

Y-PSZ at T $\gtrsim$ 700C; even at T = 23C, the Y-PSZ compressive-tensile strength ratio is $\lesssim$ three. These low ratios can be rationalized by applying yield criteria based on shear and dilatation, as outlined recently by Chen and Morel.[3]

The shear band deformation of the polycrystalline Y-PSZ takes place at a surprisingly low temperature. This suggests that with modest adjustments in loading rate, grain size, and/or confinement (to control dilatation) it might be possible to suppress shear band formation and cavitation, and achieve, in the temperature range 700-800C, the homogeneous GB sliding required for superplastic forming. Recent work by Wakai, et al,[19] has shown that superplastic flow of 0.3 μm Y-PSZ is possible at strain rates on the order of $10^{-4}s^{-1}$, but requires a temperature of at least 1450C. It will be recalled that the present Y-PSZ tetragonal grains were on the order of 0.5 μm in size, and test temperatures did not exceed 800C.

Conversely, creep resistance obviously could be improved by a large grain size, and the use of a sintering aid characterized by higher viscosity at intermediate temperatures. It would be expected that the resulting polycrystalline material would then be forced to deform by the dislocation and transformation mechanisms observed in the single crystal work.

ACKNOWLEDGEMENT

REFERENCES

1. A. G. Evans and R. M. Cannon, "Toughening of Brittle Solids by Martensitic Transformations", Acta Met., 34 [5] 761-800 (1986).

2. E. P. Butler, "Transformation-Toughened Zirconia Ceramics", Materials Science and Technology, 1 [6] 417-32 (1985).

3. I-W. Chen and P. E. R. Morel, "Implications of Transformation Plasticity in ZrO_2-Containing Ceramics: I, Shear and Dilatation Effects", J. Am. Ceram. Soc., 69 [3] 181-89 (1986).

4. M. V. Swain, "Inelastic Deformation of Mg-PSZ and Its Significance for Strength-Toughness Relationships of Zirconia Toughened Ceramics", Acta Met. 33 [11] 2083-91 (1985).

5. R. Chaim, M. Ruhle, and A. H. Heuer, "Microstructural Evolution in a ZrO_2-12 wt.% Ceramic", J. Am. Ceram. Soc., 68 [8] 427-31 (1985).

6. M. Ruhle and N. Claussen, "Microstructural Studies of Y_2O_3-Containing Tetragonal ZrO_2 Polycrystals (Y-TZP)", pp. 352-70 in Advances in Ceramics, Vol. 12, Science and Technology of Zirconia II. Edited by N. Claussen, M. Ruhle, and A. H. Heuer. American Ceramic Society, Columbus, OH, 1984.

7. A. Dominguez-Rodriguez, K. P. D. Lagerlof, and A. H. Heuer, "Plastic Deformation and Solid Solution Hardening of Y_2O_3-Stabilized ZrO_2", J. Am. Ceram. Soc., 69 [3] 281-84 (1986).

8. A. Dominguez-Rodriguez, V. Lanteri, and A. H. Heuer, "High-Temperature Precipitation Hardening of Two-Phase Y_2O_3-Partially Stabilized ZrO_2 Single Crystals: A First Report", J. Am. Ceram. Soc., 69 [3], 285-87 (1986).

9. G. Wahlberg, L. K. L. Falk, G. L. Dunlop, and K.-O. Axelsson, "The Intergranular Microstructure of a Partially Stabilized ZrO_2 Material", J. Mat. Sci. Lttrs., 4 [11], 1353-55 (1985).

10. L. J. Schioler, R. N. Katz, A. C. Gonzalez, and B. R. Lawn, "Effect of Overaging on the Room-Temperature Strength of Partially Stabilized Zirconia", Cer. Bull., 64 [2], 326-27 (1985).

11. J. Lankford, "Deformation and Fracture of Yttria-Stabilized Zirconia Single Crystals", J. Mat. Sci., 21 [6], 1981-89 (1986).

12. M. L. Mecartney, W. T. Donlon, and A. H. Heuer, "Plastic Deformation in CaO-Stabilized ZrO_2 (CSZ)", J. Mat. Sci. 15 [4], 1063-65 (1980).

13. V. Lanteri, A. H. Heuer, and T. E. Mitchell, "Tetragonal Phase in the System ZrO_2-Y_2O_3", pp. 118-30 in Advances in Ceramics, Vol. 12, Science and Technology of Zirconia II. Edited by N. Claussen, M. Ruhle, and A. H. Heuer. American Ceramic Society, Columbus, OH, 1984.

14. B. J. Dalgleish, E. B. Slamovich, and A. G. Evans, "Duality in the Creep Rupture of a Polycrystalline Ceramic", J. Am. Ceram. Soc., 68 [11] 575-81 (1985).

15. B. J. Dalgleish and A. G. Evans, "Influence of Shear Bands on Creep Rupture in Ceramics", J. Am. Ceram. Soc., 68 [1] 44-48 (1985).

16. J. W. Rudnicki and J. R. Rice, "Conditions for the Localization of deformation in Pressure-Sensitive Dilatant Materials", J. Mech. Phys. Solids, 23 [6] 371-94 (1975).

17. R. A. Page, J. Lankford, and S. Spooner, "Nucleation and Early-Stage Growth of Creep Cavities in Hot-Pressed Silicon Carbide", Acta Met., 32 [9] 1275-86 (1984).

18. J.-G. Wang and R. Raj, "Mechanism of Superplastic Flow in a Fine-Grained Ceramic Containing Some Liquid Phase", J. Am. Ceram. Soc., 67 [6] 399-409 (1984).

19. F. Wakai, S. Sakaguchi, K. Kanayama, H. Kato, and H. Onishi, "Hot Work of Yttria-Stabilized Tetragonal ZrO_2 Polycrystals", Proc. Second International Symposium on Ceramic Materials and Components for Engines, Lubeck-Travemunde, FRG, April, 1986 (in press).

II.
TEMPERATURE, STRAIN RATE, AND FIBER ORIENTATION EFFECTS IN THE COMPRESSIVE FRACTURE OF SiC FIBER-REINFORCED GLASS MATRIX COMPOSITES

J. Lankford

Southwest Research Institute
San Antonio, TX, USA

Abstract

Continuous SiC fiber-reinforced glass matrix composites have been tested in compression over a wide range in temperature and loading rate. Both uniaxial and crossplied fiber orientations were studied. Strength is found to depend sensitively on orientation and loading rate, while temperatures to 800C have less effect. Orientation effects are explained in terms of matrix microfracture and fiber buckling. The latter are shown to also control strengthening at very high (Hopkinson pressure bar) strain rates, where it is hypothesized that strength is enhanced by inertial effects which inhibit the development of the localized pockets of intense matrix microfracture and general buckling required for the nucleation of fiber kinks.

INTRODUCTION

Ceramic fiber-reinforced ceramic matrix composites are intended for applications in which they will be subjected to wide ranges in temperature, loading rate, and stress state. In order to improve the properties, and predict the lifetimes, of these complex materials, it is necessary to have a good understanding of their failure micromechanics, and how these are controlled by the interaction between composite microstructure and loading parameters.

There has developed a fairly detailed basis for modeling the tensile failure of unidirectional ceramic-fiber/ceramic matrix composites, based in particular on the recent work by Marshall and Evans.[1,2] Their model is based on the sequential development of multiple matrix cracking, fiber fracture, and finally fiber pullout; pullout is controlled by fiber-matrix friction and matrix residual stresses. Measurement of the latter parameters permits the prediction of tensile strength, although loading rate and temperature are not treated.

The case of flexural failure is considerably more complicated,[1] involving the development of both tensile and compressive damage; failure in flexure of ceramic composites has not yet been successfully modeled. Similarly, prediction of both the tensile and flexural failure of laminated ceramic matrix composites[3] is complicated by residual stresses in the laminates, and laminate cracking. Prewo has characterized[4] macroscopically the effect of temperature and layup/orientation on the tensile, flexural, and compressive strength of these materials, but the results do not (and were not intended to) provide guidelines for micromechanical modeling.

The failure of ductile-matrix unidirectional composites subject to compression has been treated fairly successfully from a theoretical standpoint,[5] and Evans and Adler[6] have analyzed the initiation of failure (kinking) in crossplied carbon-carbon composites, which can be treated as "plastic". However, the compressive failure of composites composed of either unidirectional or crossplied brittle fibers in a brittle matrix has not yet been treated analytically. It is evident that the development of instability must involve fiber buckling and kinking,[5,6] but this is necessarily controlled by yielding of the matrix. For brittle matrices, "yielding" must involve processes other than plastic flow. Similarly, any dynamic processes relevant to such failure are more likely to be controlled by inertial effects,[7,8] rather than by thermally activated plastic processes.

The present investigation is aimed at characterizing further the micromechanisms responsible for compressive damage in unidirectional and laminated ceramic fiber-ceramic matrix composites. In particular, recent research[9] involving the temperature dependence of compressive failure has now been extended to cover a wide range in loading rate as well. The strong influence of strain rate which is found is interpreted in terms of the dynamics of matrix microfracture and subsequent fiber buckling.

EXPERIMENTAL APPROACH

Materials

The materials investigated in this study were based on the incorporation of ~15 μm diameter Nikalon* SiC fibers into a glass matrix, which was ceramed by means of a post-fabrication heat treatment.[4] Composite panels of this material (COMPGLAS[TM]) were provided by the United Technologies Research Center through the Office of Naval Research. These used as their matrix the lithium-aluminosilicate known as LAS-II;[4] it has been characterized chemically and microstructurally elsewhere.[10] Panels were obtained in two layup conditions: (1) all fibers oriented essentially parallel to one another (0° orientation); (2) crossplied, using 200 μm thick laminates of parallel fibers laid up normal to one another. Both layups contained about 46 vol.% fiber, with a porosity of $\lesssim$ 1%. Although exact values of fiber and matrix strength parameters are unavailable, it is well known[1,4] that the fiber modulus, hardness, and strength are all much higher than corresponding values for the matrix.

Procedures

Specimens for compression testing were machined from the as-received panels in the form of right circular cylinders (12 mm long x 6 mm diameter). For the 0° specimens, the cylinder axis was parallel to the fibers, while for the crossplied material, two stress axis orientations were selected. In the first case, the cylinder was aligned parallel to one set of fibers, and normal to the other (0/90); in the second, the compression axis was oriented at 45° to both sets of fibers (45/45).

---

*Nippon Carbon Company, Ltd, Japan.
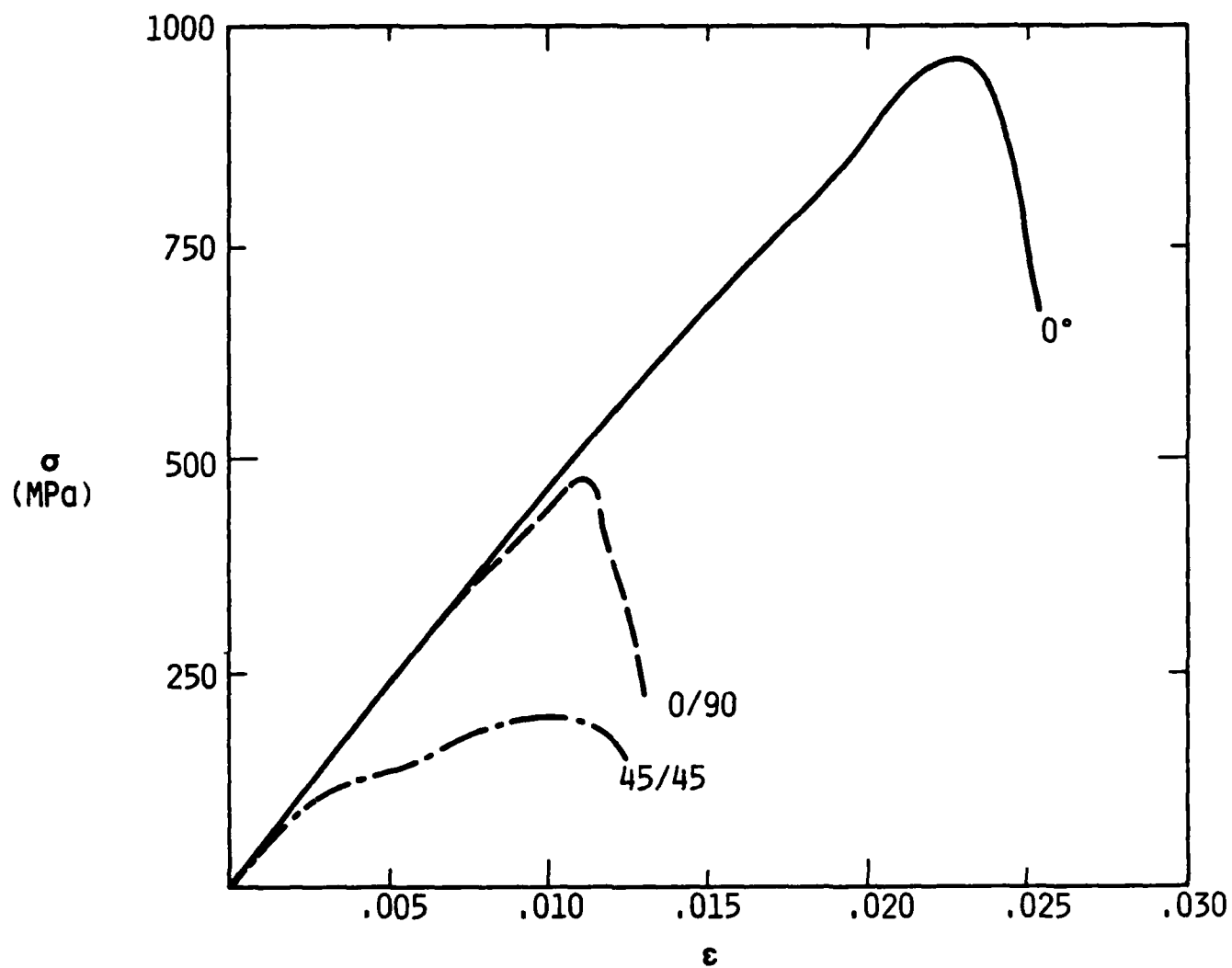
Figure 1. Stress versus strain for 0°, 0/90, and 45/45 Compglas at 23C and a strain rate of ~4s^{-1}.

All specimens were tested in air at either 23C or 800C.[9] Tests at strain rates of ~ $10^{-4}s^{-1}$ and $1s^{-1}$ were run in a standard hydraulic test machine, while rates on the order of 10^3s^{-1} were achieved by means of a split Hopkinson pressure bar. In order to prohibit brooming, small nickel-base superalloy rings were honed to just fit over the ends of each specimen.[9]

The specimen stress-strain curve was obtained by recording crosshead displacement. Concurrently, acoustic emission (AE) was monitored using a transducer resonant at 160 kHz, and attached outside the hot zone of the furnace to the alumina loading platens. At various inelastic strain levels, including post-ultimate load deformation, specimens were unloaded intact. They were then sectioned using a low speed diamond saw, carefully polished to remove any sectioning damage. Damage introduced by compressive loading was characterized by means of optical and scanning electron microscopy.

RESULTS

Stress-Strain Behavior

Typical stress (σ)-strain (ε) curves for SiC-LAS-II specimens compressed at room temperature are shown in Figure 1. Results shown are for a strain rate ($\dot{\varepsilon}$) of about $4s^{-1}$; qualitatively similar results are found for lower strain rates, and for temperatures as high as 800C. Basically, the specimens yielded, i.e., the σ-ε curve deviated from its elastic loading line, well below the ultimate strength (σ_f). Following yield (σ_y), the material "hardened", and after the attainment of ultimate, the stress tended to drop off stably, as shown in Figure 1. It was observed that the

threshold stress for acoustic emission (σ_{AE}) was always well below the yield strength (tests at $\dot{\varepsilon} > 10^{-4}s^{-1}$ were too fast to permit the processing of AE data).

These results are summarized in Table I, in which it can be seen that the plastic strain-at-failure ($\varepsilon_p{}^f$) ranged from zero (pressure bar tests) to 0.0178. Ductility was greatest for the 45/45 orientation, with ε_p averaging ~ 0.01 for $\dot{\varepsilon} < 10^3s^{-1}$. Furthermore, it is interesting to note that the strain-to-failure is considerably greater at $\dot{\varepsilon} \simeq 2s^{-1}$ than it is at $\dot{\varepsilon} \simeq 10^{-4}s^{-1}$.

At 23C, it was found that strain rate had little effect on σ-ε behavior, as shown in Figure 2. However, the apparent modulus at 800C increases significantly upon changing the strain rate from $1.9 \times 10^{-4}s^{-1}$ to $4.4s^{-1}$ (Figure 3). At strain rates on the order of 10^3, the stress-strain curve was essentially elastic to failure, with no noticeable change in modulus.

Strength

Ultimate compressive strength as a function of strain rate at 23C and 800C is shown for 0°, 0/90, and 45/45 layups in Figures 4, 5, and 6, respectively. It is evident upon comparing the three figures that the 0° composite is by far the strongest. At 23C, there is little strain rate dependence in σ_f until $\dot{\varepsilon} \gtrsim 2s^{-1}$, above which there is a dramatic increase in strength. At 800C, on the other hand, σ_f appears to increase steadily, but only gradually, over the entire seven decades in strain rate.

For the 0/90 configuration (Figure 5) there is no temperature dependence for $\dot{\varepsilon} \lesssim 4s^{-1}$, but above this limit, there is a tendency for σ_f to increase rapidly with $\dot{\varepsilon}$. For this test series, an effort was

TABLE I

MECHANICAL BEHAVIOR

Layup	T(°C)	$\dot{\varepsilon}(s^{-1})$	σ_{AE}(MPa)	σ_y(MPa)	σ_f(MPa)	ε_p
0°	23	6×10^{-5}	387	763	957	0.0024
0°	23	6×10^{-5}	543	755	976	0.0017
0°	23	6×10^{-5}	487	760	907	0.0025
0°	23	1.94	–	931	963	0.010
0°	23	10^3	–	–	1365	–
0°	23	10^3	–	–	1787	–
0°	23	10^3	–	–	2125	–
0°	800	6×10^{-5}	697	856	1132	0.0008
0°	800	5.0	–	966	1240	0.002
0°	800	10^3	–	–	1408	–
0°	800	10^3	–	–	1566	–
0/90	23	6×10^{-5}	–	–	304	–
0/90	23	1.2×10^{-4}	267	347	373	0.0005
0/90	23	3.3	–	–	455	–
0/90	23	3.3	–	313	474	0.0008
0/90	23	1.9×10^3	–	–	971	–
0/90	23	1.9×10^3	–	–	973	–
0/90	23	0.57×10^3	–	–	490	–
0/90	23	0.64×10^3	–	–	565	–
0/90	800	1.2×10^{-4}	283	353	353	0.004
0/90	800	2.0	–	370	375	0.01
0/90	800	2.7×10^3	–	–	1070	–
0/90	800	2.7×10^3	–	–	1139	–
0/90	800	0.32×10^3	–	–	916	–
45/45	23	1.4×10^{-4}	–	95	185	0.0155
45/45	23	1.6	–	104	199	0.0078
45/45	23	1.8	–	104	222	0.0178
45/45	23	10^3	–	–	354	–
45/45	23	10^3	–	–	372	–
45/45	800	1.4×10^{-4}	60	108	160	0.0108
45/45	800	4.4	–	77	198	0.0112
45/45	800	10^3	–	–	311	–
45/45	800	10^3	–	–	321	–

Figure 2. Stress versus strain for 45/45 Compglas at 23C for strain rates of $3.7s^{-1}$ and $1.9 \times 10^{-4} s^{-1}$.

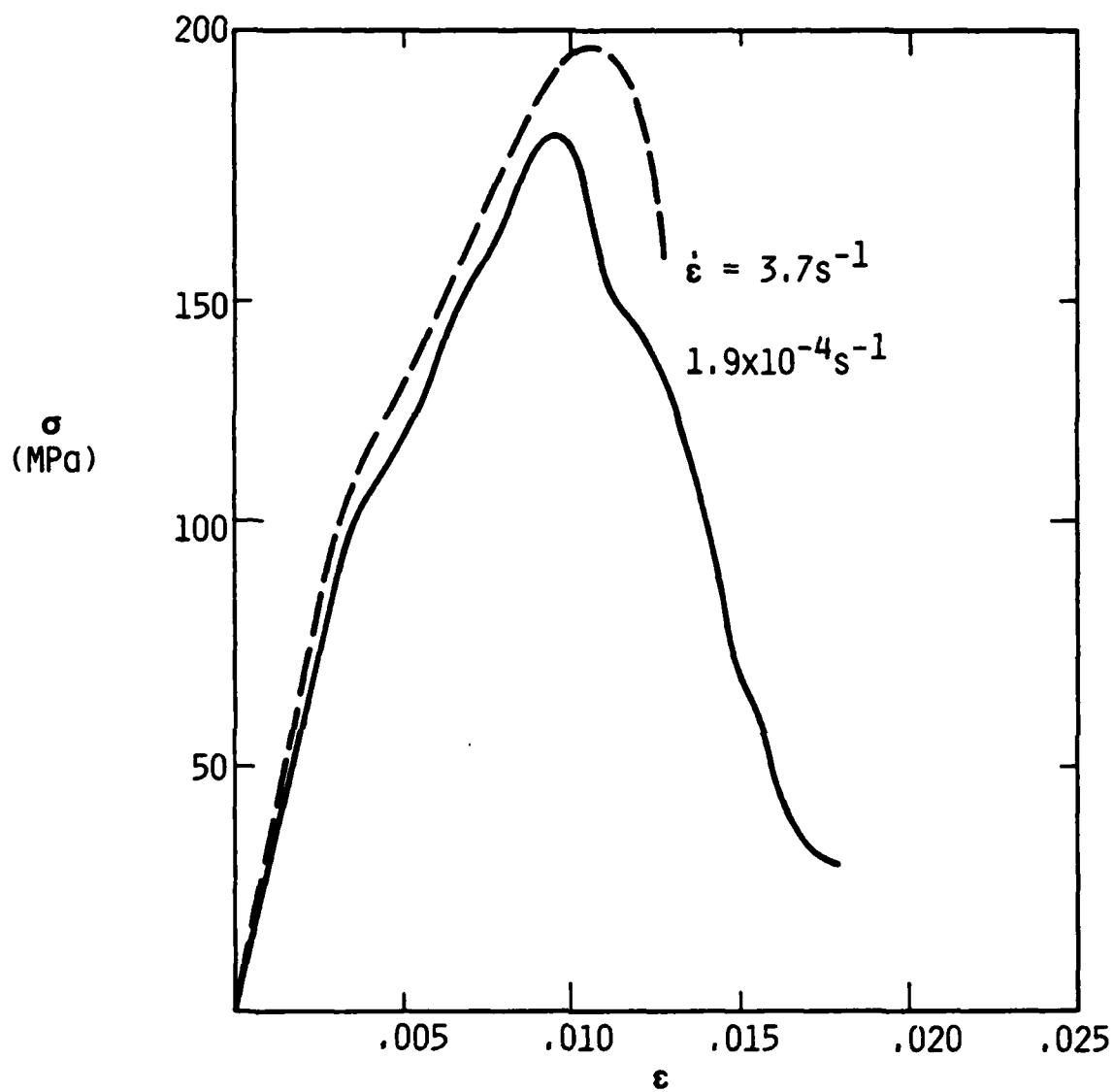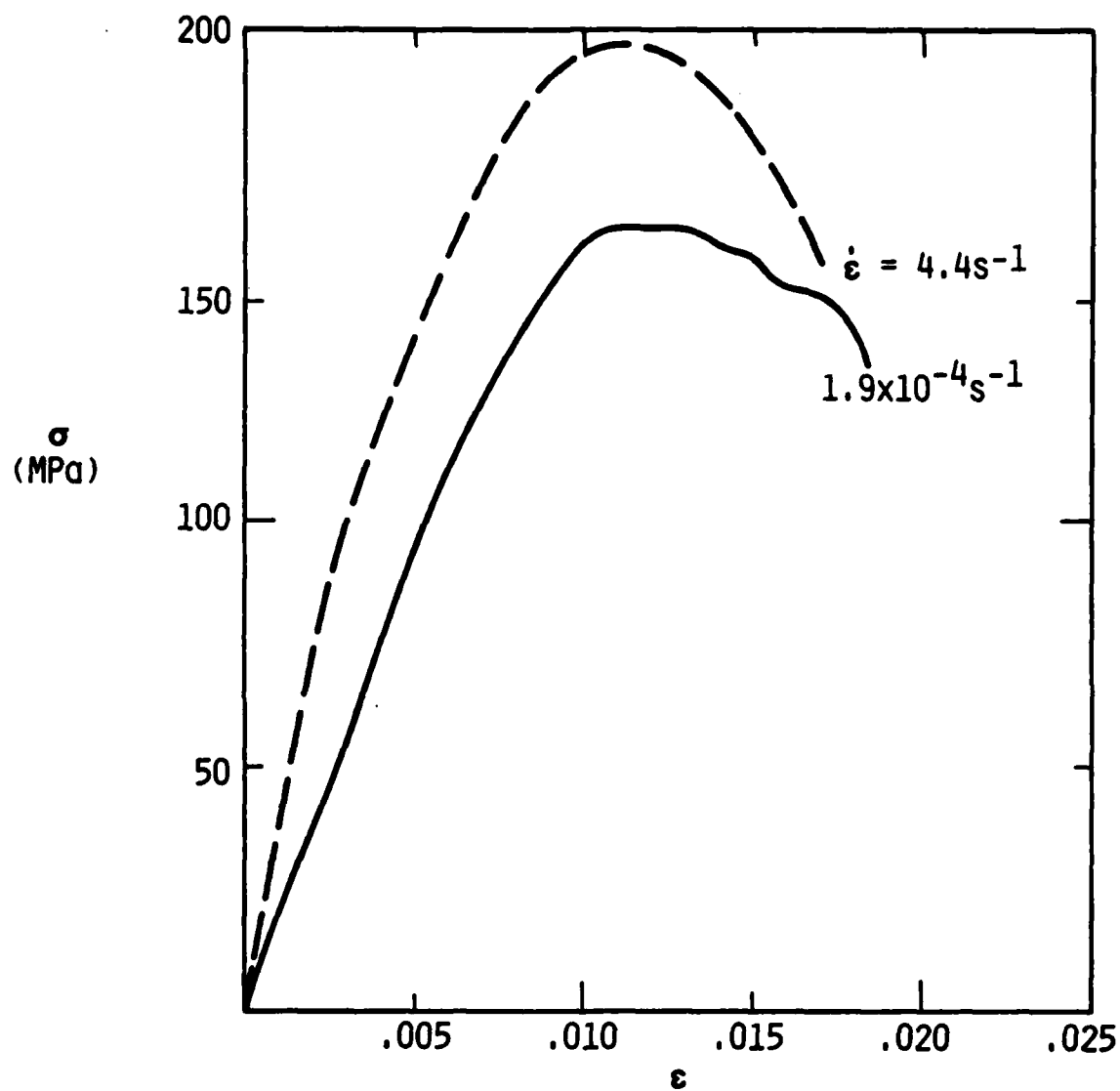**Figure 3.** Stress versus strain for 45/45 Compglas at 800C for strain rates of $4.4s^{-1}$ and $1.9 \times 10^{-4}s^{-1}$.
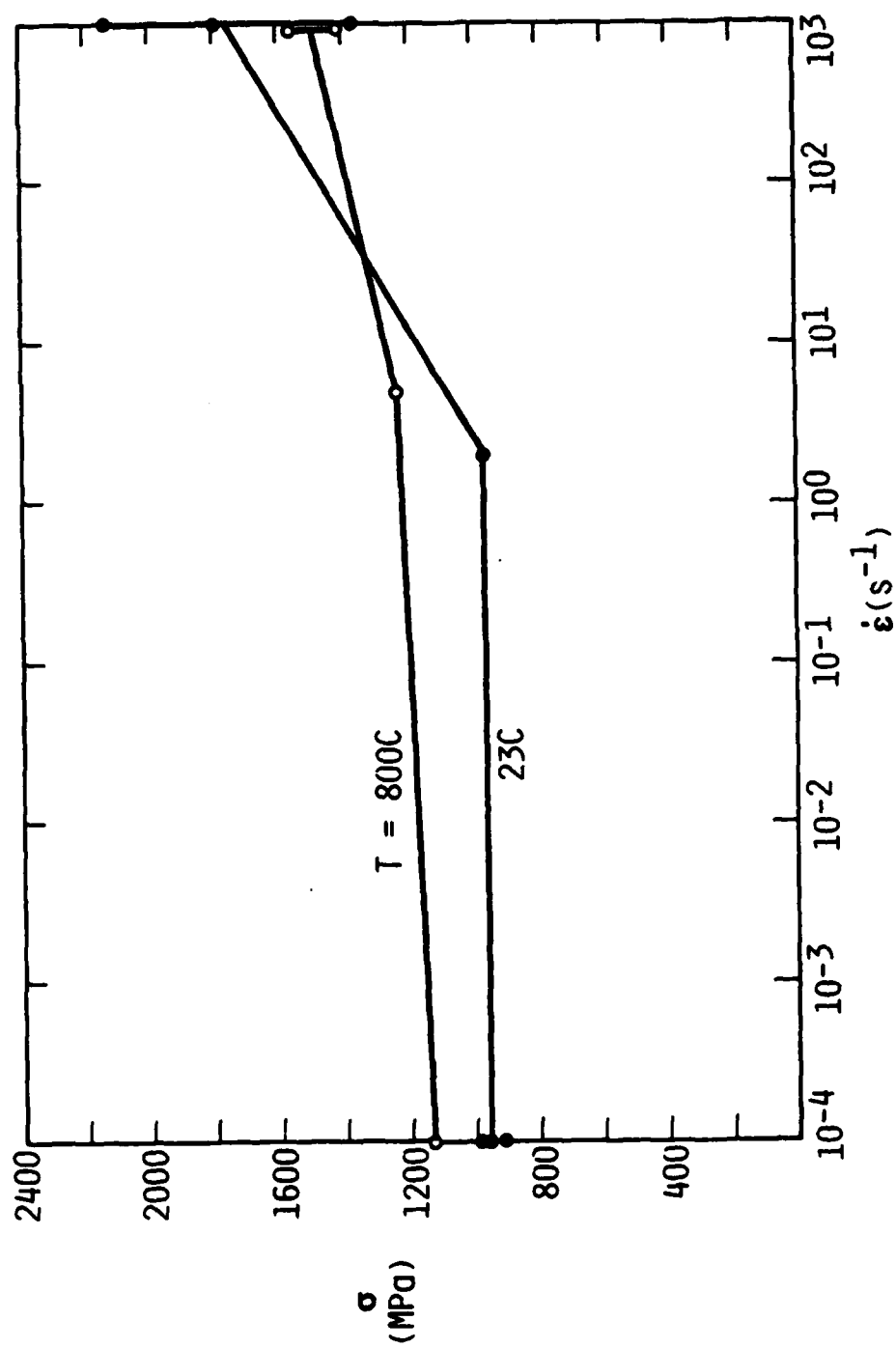
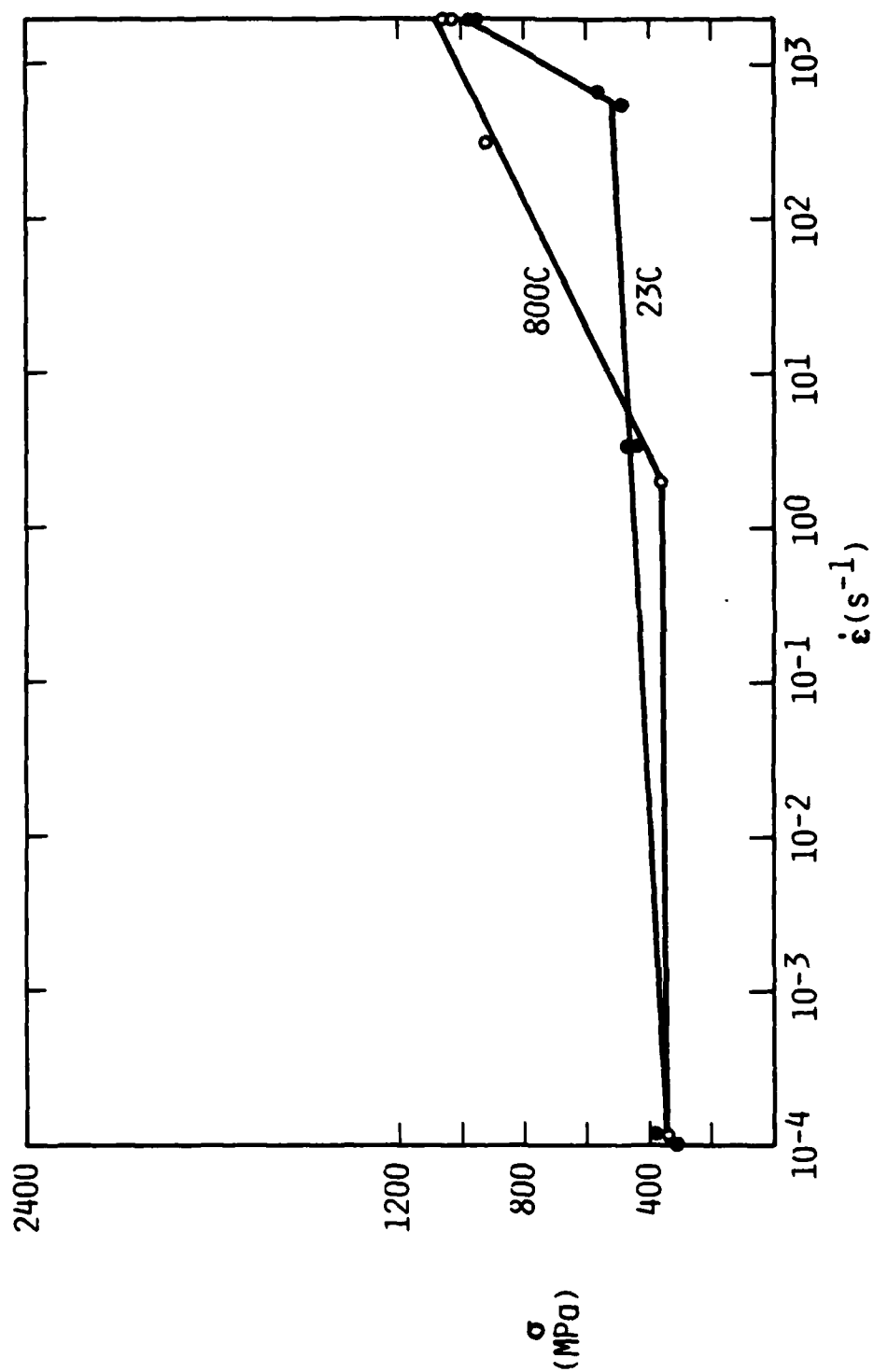Figure 4. Failure strength versus strain rate for 0° Compglas at 23C and 800C.

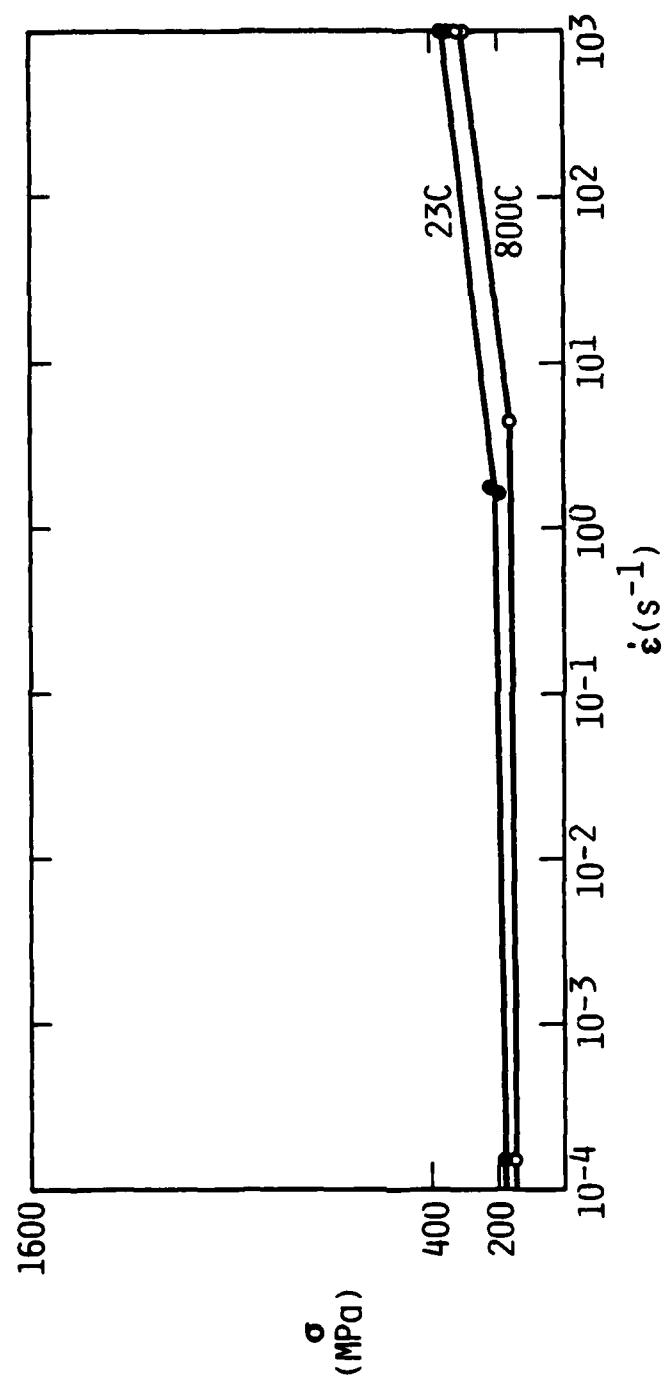Figure 5.   Failure strength versus strain rate for 0/90 Compglas at 23C and 800C.

Figure 6. Failure strength versus strain rate for 45/45 Compglas at 23C and 800C.

made to back off on the pressure bar loading rate, in order to get a better estimate of the σ_f-$\dot{\varepsilon}$ dependence in the rate sensitive regime. By this means, it was established that for $\dot{\varepsilon} \gtrsim 4s^{-1}$, $\sigma_f \propto \dot{\varepsilon}^{.16}$ at 800C, while at 23C, $\sigma_f \propto \dot{\varepsilon}^{.48}$. Over the range $4s^{-1} < \dot{\varepsilon} < 10^3 s^{-1}$, the strengths at both temperatures essentially triple.

Failure strength of the 45/45 layup is basically independent of temperature over the entire range in $\dot{\varepsilon}$ (Figure 6). However, σ_f does approximately double between $\dot{\varepsilon} \approx 2s^{-1}$ and $\dot{\varepsilon} = 10^3 s^{-1}$. The exact rate of strength increase in this range would require further pressure bar experiments at lower loading rates. It should be noted that the strength of the 45/45 configuration under dynamic loading conditions (~ 375 MPa) is nearly equal to that of the 0/90 layup at lower strain rates.

Failure Micromechanics

Before attempting to interpret the preceding experimental results, it is helpful to briefly review the basic failure mechanisms as determined earlier[9] in compression tests performing at low loading rates. In summary, it was concluded that σ_{AE} corresponds to the threshold stress level for the nucleation of axial matrix microcracks. For 0° COMPGLAS, this nucleation is a measure of the intrinsic resistance of the glass matrix to compressive loading. However, for layups with fiber laminates oriented at 90° or 45° relative to the stress axis, matrix crack initiation occurs via SiC fiber "indentation" of the glass-ceramic separating the fibers. Regardless of the mode of initiation of matrix microcracks, at some higher stress level, they will begin to link up into axial macrocracks. At this "yield" stress, σ_y, the composite modulus begins to decrease due to fiber flexure, i.e., buckling. Ultimate failure corresponds to the kinking of

buckled fibers, which is facilitated in 0°-plies in laminated material by the linking, via shear, of matrix macrocracks in adjoining laminates composed of fibers oriented at either 45° or 90° to the stress axis.

Examples of this process, and the attendant kinking associated with failure, are shown in Figures 7a and 7b, where it can be seen that the same fundamental process obtains at both 23C and 800C. It is evident that macroscopic axial cracks have formed in each 90° laminate, and that they have yielded locally in shear to produce kinks in adjacent 0° laminates as indicated by the arrows.

At higher loading rates, this scenario is altered, as shown in Figure 7c. This section was obtained from a specimen loaded in the Hopkinson pressure bar at $\dot{\epsilon} = 10^3 s^{-1}$ to approximately the same stress level as the specimens corresponding to Figures 7a and 7b. The former specimen did not fail, and the only damage present is in the outer fiber of the sample, which appears to have begun to buckle, but has not formed a kink. The macroscopically uncracked bulk interior contrasts vividly witn the sections through the lower strain rate specimens (Figures 7a and 7b).

In order to understand the basis for this difference, it is helpful to consider how buckling and kinking is accommodated in a damaged specimen. An example of this is shown in Figure 8, which corresponds to the central region of Figure 7b. It can be seen that the glass matrix has essentially been reduced to rubble by the formation of numerous extremely fine-scale fragments, many on the order of a few micrometers in minimum dimension (the dark material between the fragments is the polymeric binder with which the specimen was infiltrated prior to sectioning). Furthermore, in order to accommodate the imposed shear displacement which has
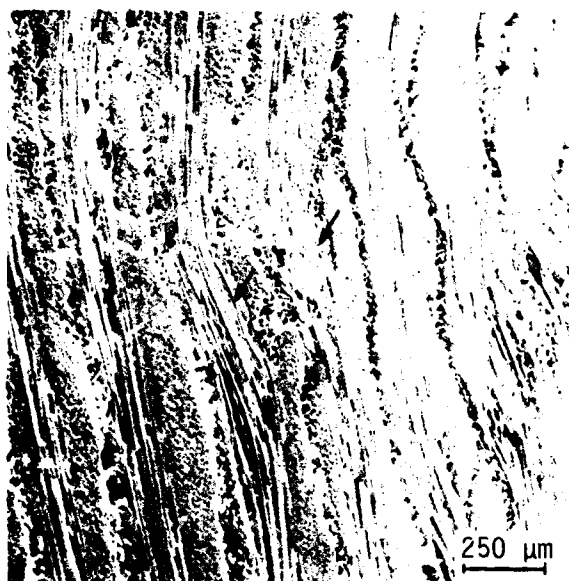
(a) $\dot{\varepsilon} = 1.2\times10^{-4}s^{-1}$, T = 23C; arrows indicate severe kinking. Axial fracture throughout volume in 90° laminates.
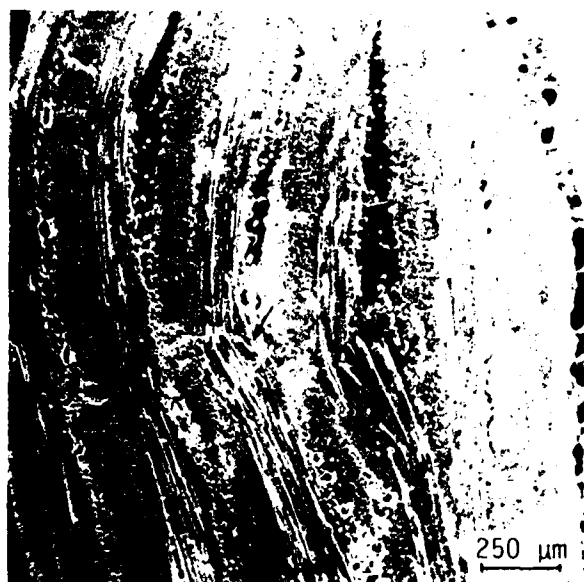
(b) $\dot{\varepsilon} = 1.2\times10^{-4}s^{-1}$, T = 800C; arrows indicate severe kinking. Axial fracture throughout volume in 90° laminates.

(c) $\dot{\varepsilon} = 10^{3}s^{-1}$, T = 23C; specimen is unfailed, but stressed above σ_f for $\dot{\varepsilon} = 10^{-4}s^{-1}$. Axial fracture only in outermost 90° laminate.

Figure 7. Damage in 0/90 laminates at various temperatures and loading rates. Stress axis is vertical. Left side of each photomicrograph is near outside of specimen, right side is near centerline.

Figure 8. Higher magnification view of center of Figure 7(b). Note fracture of inter-fiber matrix into many extremely fine fragments, which slide relative to one another to accommodate fiber rotation. Stress axis is vertical.

kinked the fibers, the matrix fragments have slid and rotated relative to one another. Visible in the 90° laminate to the right of the kink is a macroscopic axial crack made up of fiber-matrix interface cracks linked up with fiber-nucleated matrix "indent" cracks. Such features are common throughout the bulk of specimens deformed for all temperatures, and for all $\dot{\varepsilon} \lesssim 10s^{-1}$.

For rapid loading, the situation is as shown in Figure 9. The outer 0° ply has delaminated via crack formation and linkup in the adjacent 90° ply (Figure 9a); buckling is accommodated by local matrix fragmentation and fragment sliding/rotation. However, near the next 0° bundle, only a small zone of concentrated matrix microfracture can be found (Figure 9b). The damage is insufficient to produce a macroscopic axial crack, hence no buckling has occurred. Elsewhere in the specimen (Figure 9c), only isolated 90° fiber-to-fiber cracks are present; although their density is uniform and fairly high, they have not experienced conditions sufficient to cause macroscopic linkup.

DISCUSSION

Fiber Orientation

The dependence of strength upon layup configuration/orientation (Figure 1) can be rationalized essentially on the basis of the relative ease of nucleating matrix microcracks, since they are necessary in order for fiber buckling and kinking to occur. It is apparent from Table I that σ_{AE}, the stress level for nucleating matrix cracks, is highest for 0° unidirectional layups, less for 0/90 laminates, and still lower for 45/45
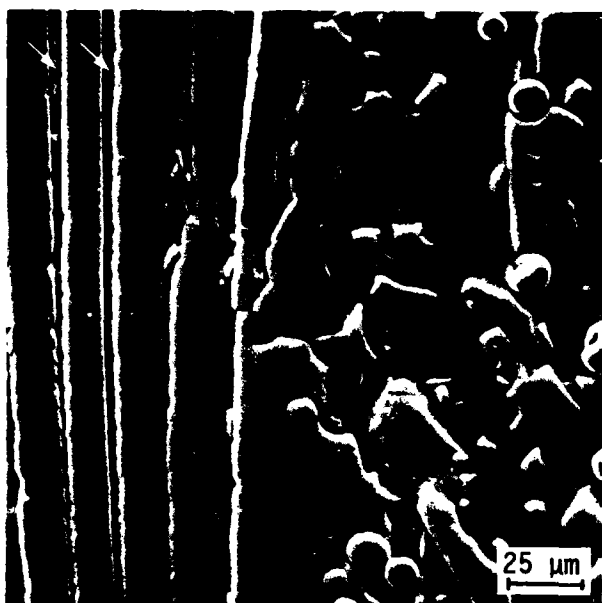
(a) Matrix microfracture near outer 0° ply accommodating fiber buckling, as evidenced by fiber rotation/separation (arrows).
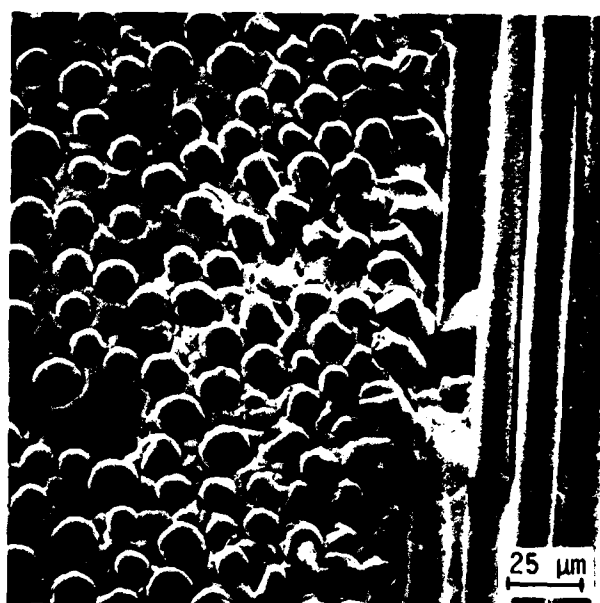
(b) Localized concentrated micro-fracture in matrix near second (from outer surface) set of 0° plies. Damage is insufficient to cause buckling.
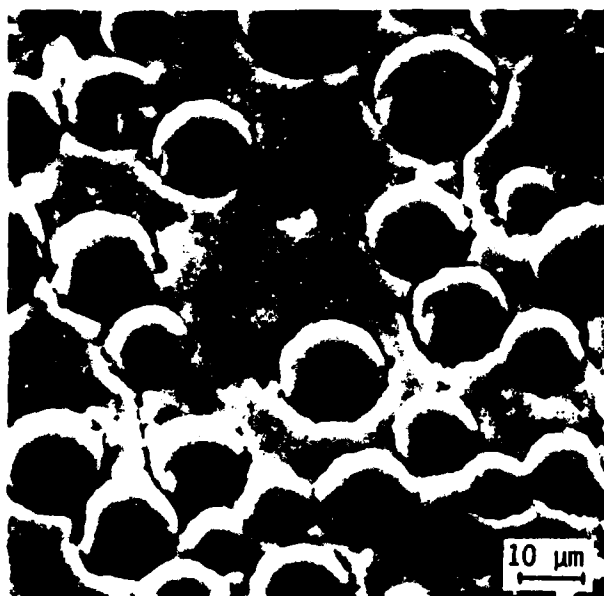
(c) Matrix microfracture caused by 90° fiber interactions in bulk of specimen.

Figure 9. Damage gradient across Figure 7(c); $\dot{\varepsilon} = 10^3 s^{-1}$, T = 23C. Stress axis is vertical.

composites. The difference between the 0/90 and 45/45 cases can be related to the fact that in the latter arrangement, every ply in the layup contains a family of SiC fiber capable of generating matrix "indentation" cracks. For the 0/90 laminates, however, only every other ply is so oriented, with the result that the stiff, uncracked 0° laminates provide support to their fractured 90° neighbors; no such support is available in the 45/45 layups. However, once matrix cracks have formed and begin to link up in the 90° plies, buckling and failure via kinking is inevitable, and will occur at a lower stress level than for the 0° unidirectional composites, whose matrix cracks, as noted earlier, are forced to nucleate at some higher intrinsic matrix strength level. On this basis, it is clearly reasonable for ultimate strength to decrease in the order 0°, 0/90, and 45/45.

The tendency for load bearing capacity to drop off stably following the attainment of ultimate strength can be laid to laminate kinking. As seen in Figures 7a and 7b, buckling eventually fills the gage section, which corresponds to the ultimate stress. Subsequently, kinking occurs stochastically at local sites, so that the deformation process proceeds at incrementally reduced stress levels.

In order to appreciate the role of matrix microfracture in the kinking process, and to justify the rationale proposed above for ordering the layup/orientation dependence of compressive strength, it is helpful to consider the model set forth by Evans and Adler[6] pertaining to kinking in three-dimensional composites capable of some plastic flow. In the model, it is envisaged that tensile fiber stresses are generated by compressive shear displacements, such as the pre-kink buckling observed in the present

instance. Analysis of the micromechanics of the problem leads to the conclusion that the critical compressive stress for buckling σ_c is related to the composite material parameters according to

$$\frac{S_0}{\sigma_{ym}} = \left(\frac{\sigma_c}{\sigma_{ym}}\right)^{1-3m} \left[\frac{3\pi\lambda wc}{2} \ln \frac{3\pi^2}{\omega}\left(\frac{\sigma_c}{\sigma_{ym}}\right)^2\right]^{1/m}$$

where S_0 and m are fiber strength and strength distribution parameters, respectively; σ_{ym} is the matrix yield strength; λ is a constant; w is the kink width; c is the fiber radius, and ω is a stiffness factor.

Inspection of this equation shows that σ_c depends mainly on the matrix yield strength, and on S_0 and m. Since S_0 and m should be essentially independent of layup configuration and orientation relative to the compressive stress axis, layup/orientation dependence must arise principally from σ_{ym}. Clearly, the present glass matrix does not yield plastically; rather, it fragments, creating a shear instability capable of accommodating a kink via the sliding and rotation ("flow") of the fragments (Figure 8). The level of σ_{ym} depends on the relative ease of nucleating matrix microcracks, which depends on fiber orientation as outlined above.

Influence of Temperature

The σ-ε results shown in Figures 2 and 3 reflect an important factor, i.e., the softening of the glass matrix thought[10] to occur at elevated temperature (800-1000C). At 23C, the rate of loading has little effect on material stiffness (Figure 2), while at 800C, increased $\dot{\varepsilon}$ is very effective in defeating the softening which manifests itself at low

strain rate (Figure 3). This softening may account for the increase in strength with temperature for 0° COMPGLAS at $\dot{\varepsilon} \gtrsim 10^1$, shown in Figure 4. Matrix cracks are nucleated in this material due to resolution of the applied compressive stress into multiple localized multiaxial stress fields whose tensile components are roughly normal to the axis. Sites where this takes place include pores, grain boundaries, and regions of modulus mismatch. By softening in such locales, the matrix can minimize the level of the induced tensile stress, thereby requiring a higher applied compressive stress in order to produce failure, as observed.

For 0/90 and 45/45 laminates, on the other hand, matrix microfracture is caused solely by the stress concentration produced by the indentation fields of adjacent SiC fibers. Thermally-induced matrix softening is unlikely to reduce these intense local stress fields sufficiently to significantly alter indentation microfracture (at least for the intermediate temperature range covered in this study), as reflected in the relative temperature independence of σ_f for 0/90 and 45/45 laminates observed for $\dot{\varepsilon} \gtrsim 10^1$ (Figures 5 and 6).

Influence of Strain Rate

The influence of rapid loading rate on ultimate strength is remarkably powerful (Figures 4-6), and its basis may be somewhat more complicated than that found in monolithic ceramics[7,8,11] and geologic materials.[7,12] For the latter, it has been demonstrated that above a critical, material-dependent strain rate on the order of $10^3 s^{-1}$, inertial

effects can minimize the extension of microcracks, and thereby generate significant strengthening. Linear elastic dynamic fracture mechanics analysis indicates[7] that above the critical strain rate, the stress to activate a flaw will be given by

$$\sigma_c \simeq A\left(\frac{E\ K_{IC}^2}{c}\right)\dot\epsilon^{.33}$$

where E is the elastic modulus, K_{IC} is the fracture toughness, and c is the shear velocity of the material. In agreement with this prediction, previous experiments on SiC, Si_3N_4, Al_2O_3,[11] and limestone[12] have shown that indeed, for strain rates in the range of 10^3s^{-1}, $\sigma_c \tilde\alpha\ \dot\epsilon^{.33}$.

The present results on SiC-reinforced glass support this general trend. However, the data on the 0/90 layups show several unusual patterns of behavior. First, the upturn in the σ_f-$\dot\epsilon$ curve for T = 800C occurs at far too low a strain rate ($\sim 2s^{-1}$) to be ascribed to inertial effects. Furthermore, while at 23C the transition to inertial control takes place as expected, i.e., at $\dot\epsilon \simeq 10^3s^{-1}$, subsequently $\sigma_f\alpha\ \dot\epsilon^{.48}$. The latter strain rate exponent represents strengthening in excess of that predicted by microcrack inertia alone.

Insufficient variation in experimental strain rates precludes similar conclusions regarding the precise form of the dependence of σ_c upon $\dot\epsilon$ in the range $\dot\epsilon \simeq 10^3s^{-1}$ for the 45/45 layups at 23C and 800C, and the 0° unidirectional composite at 23C. However, the results of the 0° tests at 800C suggest that the strength was increasing steadily over the entire strain rate range, and that any transition to the inertia-controlled regime was, at best, just beginning at $\dot\epsilon = 10^3s^{-1}$. This would

imply that the 800C, 0/90 σ_f-$\dot\varepsilon$ curve (Figure 5) is actually the product of two independent strengthening mechanisms, one acting over a broad range in $\dot\varepsilon$, and effective only at elevated temperatures, and the other operative only under dynamic loading conditions, essentially independent of temperature.[8] This hypothesis can be rationalized by considering the relevant failure micromechanisms, as follows.

In order for failure to occur, two things (at least) must happen: (1) matrix microcracks must nucleate and coalesce, a process subject to inertial control;[7] (2) the composite (or parts of it) must buckle, a process controlled by the stiffness of the matrix supporting the strengthening fibers. Specifically, for the shear-type buckling which predominates in the present case, buckling is directly controlled by the shear modulus of the matrix (G_m) according to[13]

$$\sigma_b = \frac{G_m}{1-v_f}$$

where σ_b is the critical stress to cause buckling instability, and v_f is the fiber volume fraction. The matrix stiffness naturally tends to be reduced at elevated temperature, but can be restored by increasing the strain rate, as demonstrated in Figure 3. Thus, as the loading rate increases for tests at 800C (Figure 4), the matrix modulus increases as well, and it becomes more difficult, i.e., requires higher applied stresses, for buckling fibers to reach the critical radius required for kinking (failure). This beneficial effect would not obtain at 23C (Figure 2), which probably is reflected in the very flat σ_f-$\dot\varepsilon$ curves of Figures 4 and 5 (it is likely that the curve for $\dot\varepsilon > 10^0 s^{-1}$ in Figure 4 is incorrect

as drawn, and that further tests at strain rates just below $10^3 s^{-1}$ would show essentially the same sort of inertial strengthening found in the 0/90 material at 23C).

The fact that $\sigma_f \propto \dot{\varepsilon}^{.48}$ for the 23C, 0/90 tests at $\dot{\varepsilon} \approx 10^3 s^{-1}$ suggests that in addition to inertia-controlled microfracture, inertial effects involving buckling may also be contributing to the strain rate strengthening. Recalling Figures 7c and 9, it is evident that buckling in the center section of the specimen is controlled by the speed with which a buckling "front" can progress from the surface to the interior. It is likewise evident that this process cannot take place prior to fairly extensive matrix microfracture and microcrack coalescence. Finally, buckling in the specimen interior is required for failure, since observational evidence indicates that kinking (failure) occurs near the specimen center section (Figures 7a and 7b). Superposition of these two rate-sensitive processes therefore may account for the strain rate exponent of 0.48 measured in the 0/90 experiments at 23C, versus the value of 0.33 predicted theoretically[7] for matrix microfracture alone.

CONCLUDING REMARKS

It is apparent that the compressive failure of fiber-reinforced glass matrix composites is a complex process. Efforts to model it must take into account the sequential development of compressive damage specifically, and its dependence upon fiber layup configuration, orientation relative to the compressive axis, temperature, and loading. Although the stress-strain curves for these materials tested in compression qualitatively, and in some cases quantitatively, resemble those obtained for

tensile loading,[1] the relevant damage and failure mechanisms are funda-
mentally different. Whereas tensile/flexural failure involves[1,3] matrix
microfracture, fiber pullout, fiber fracture, and delamination fracture,
compressive failure occurs via matrix microstructure (including fiber
indentation-induced cracking), fiber buckling, and fiber (bundle) kink-
ing. Elevated temperatures degrade composites subject to tensile stresses
by means of fiber weakening and increasing the fiber-matrix interfacial
shear strength,[14] which increases the tendency for fibers to break rather
than pull out. Conversely, the same temperatures under compressive load-
ing relax local tensile stress concentrations, suppressing crack nucle-
ation, but at the same time reduce matrix stiffness, thereby facilitating
fiber (bundle) buckling. The effect of rapid loading rate on tensile
failure has not been established, but the same inertial strengthening due
to suppression of microcrack extension during compression should pre-
vail.[7] However, buckling inertia would not be a factor in tensile load-
ing, as it is for compression.

Plies oriented normal to the compression axis are extremely detri-
mental to compressive strength. Further tests at higher loading rates are
required in order to establish the strain rate threshold (if one exists)
for strengthening via inertial suppression of fiber indentation matrix
microfracture.

ACKNOWLEDGEMENT

REFERENCES

1.   Marshall, D. B. and Evans, A. G., "Failure Mechanisms in Ceramic-Fiber/Ceramic-Matrix Composites", Journal of the American Ceramic Society, Vol. 68, No. 5 (1985) pp. 225-231.

2.   Marshall, D. B. and Evans, A. G., "Application of Fracture Mechanics to Fiber Composites", Ceramic Engineering and Science Proceedings, Vol. 6, Nos. 7-8 (1985) pp. 537-549.

3.   Sbaizero, O. and Evans, A. .G., "Tensile and Shear Properties of Laminated Ceramic Matrix Composites", Journal of the American Ceramic Society, Vol. 69, No. 6 (1986) pp. 481-486.

4.   Prewo, K. M., "Advanced Characterization of SiC Fiber Reinforced Glass-Ceramic Matrix Composites", ONR Technical Report, Contract No. N00014-81-C-0571 (June 1983).

5.   Piggott, M. R., "A Theoretical Framework for the Compressive Properties of Aligned Fibre Composites", Journal of Material Science, Vol. 16, No. 10 (1981) pp. 2837-2845.

6.   Evans, A. G. and Adler, W. F., "Kinking as a Mode of Structural Degradation in Carbon Fiber Composites", Acta Metallurgica, Vol. 26, No. 5 (1978) pp. 725-738.

7.   Kipp, M. E., Grady, D. E., and Chen, E. P., "Strain-Rate Dependent Fracture Initiation", International Journal of Fracture, Vol. 16, No. 4 (1980) pp. 471-478.

8.   Lankford, J., "Inertia as a Factor in the Dynamic Strength of Brittle Materials", Journal of the American Ceramic Society, Vol. 65, No. 8 (1982) p. C-122.

9. Lankford, J., "Compressive Strength and Damage Mechanisms in a SiC-Fiber Reinforced Glass-Ceramic Matrix Composite", Proceedings of the Fifth International Conference on Composite Materials (ICCMV), eds. W. C. Harrigan, J. Strife, and A. K. Dhingra, TMS-AIME, Warrendale, PA (1985) pp. 587-602.

10. Prewo, K. M., Layden, G. K., Minford, E. J., and Brennan, J. J., "Advanced Characterization of Silicon Carbide Fiber Reinforced Glass-Ceramic Matrix Composites", ONR Technical Report, Contract No. N00014-81-C-0571 (June 1985).

11. Lankford, J., "The Role of Subcritical Tensile Microfracture Processes in Compression Failure of Ceramics", Fracture Mechanics of Ceramics, Vol. 5, Ed. R. C. Bradt, A. G. Evans, D. P. H. Hasselman, and F. F. Lange, Plenum Press, NY (1983), pp. 625-637.

12. Lankford, J., "The Role of Tensile Microfracture in the Strain Rate Dependence of Compressive Strength of fine-Grained Limestone - Analogy With Strong Ceramics", International Journal of Rock Mechanics, Mining Science, and Geomechanics Abstracts, Vol. 18, No. 2 (1981) pp. 173-175.

13. Rosen, B. W., "Mechanics of Composite Strengthening", Fiber Composite Materials, American Society for Metals, Metals Park, OH (1965) pp. 37-73.

14. Luh, E. Y., and Evans, A. G., "High Temperature Failure of a SiC Fiber-Reinforced Lithium Aluminosilicate Glass Ceramic", Ceramic Engineering and Science Proceedings, Vol. 6, Nos. 7-8 (1985) pp. 608-611.

END

10-86

DTIC